https://doi.org/10.5194/gmd-2020-41
Preprint. Discussion started: 18 May 2020

Geoscientific Model Development Discussions

Implementation and assessment of a carbonate system model (Eco3M-CarbOx v1.1) in a highly-dynamic Mediterranean coastal site (Bay of Marseille, France).

Katixa Lajaunie-Salla[1], Frédéric Diaz[1], Cathy Wimart-Rousseau[1], Thibaut Wagener[1], Dominique Lefèvre[1], Christophe Yohia[2], Irène Remy-Xueref[3], Brian Nathan[3], Alexandre Armengaud[4], Christel Pinazo[1]

[1]Aix Marseille Univ., Université de Toulon, CNRS, IRD, MIO, UM 110, 13288, Marseille, France
[2]Aix Marseille Univ., CNRS, IRD, OSU Institut Pythéas, 13288, Marseille, France
[3]Aix Marseille Univ., Université d'Avignon, CNRS, IRD, IMBE, Marseille, France
[4]AtmoSud : Observatoire de la qualité de l'air en région Sud Provence Alpes Côte d'Azur, le Noilly Paradis, 146 Rue Paradis, 13294 Marseille, Cedex 06, France

Correspondence to: Katixa Lajaunie-Salla (katixa.lajaunie-salla@mio.osupytheas.fr), Frédéric Diaz (frederic.diaz@mio.osupytheas.fr)

Abstract. The Bay of Marseille (BoM, France) is impacted by the urbanized and industrialized Aix-Marseille Metropolis, which is subject to significant increases in anthropogenic emissions of CO_2. A carbonate chemistry balance module has been implemented into a biogeochemical model of the planktonic food web. The resulting model, named Eco3M-CarbOx includes 22 states variables that are dispatched into 5 compartments: phytoplankton, heterotrophic bacteria, detritus, dissolved organic and inorganic matter.

The model suggests that the variability of the dissolved inorganic carbon system is mainly driven by the seawater temperature dynamics. A seasonal trend is identified by the model and it shows that, during the mixed water column period, the BoM is a sink for atmospheric CO_2 and a net autotroph ecosystem, while during stratified water column period, the BoM is a source of CO_2 to the atmosphere and a net heterotroph ecosystem. External forcings have an important impact on the carbonate equilibrium. Wind events change seawater temperature quickly, as during upwelling, for which the BoM waters change within a few days from a source of CO_2 to the atmosphere to a sink into the ocean. Moreover, the higher the wind speed is, the higher the air-sea CO_2 gas exchange fluxes are. The river intrusions with nitrate and alkalinity supplies lead to a decrease in the pCO_2 value, favoring the conditions of a sink of atmospheric CO_2 into the BoM. The nearby highly urbanized environment of the Aix-Marseille metropolis produces strong atmospheric values of CO_2, also favoring the conditions of a sink of atmospheric CO_2 into the waters of the BoM.

1. Introduction

Current climate change mostly originates from the carbon dioxide (CO_2) increase in the atmosphere at a high annual rate (+2.63 ppm from 2018, May to 2019, May, https://www.esrl.noaa.gov/gmd/ccgg/trends/global.html). This atmospheric CO_2 increase impacts the carbonate chemistry equilibrium of the oceanic water column (Allen et al., 2009; Matthews et al., 2009). Oceans are known to act as a sink for anthropogenic CO_2, *i.e.* 30% of emissions, which leads to a marine acidification (Gruber et al., 2019; Orr et al., 2005; Le Quéré et al., 2018).

CO_2 is a key molecule in the biogeochemical functioning of the marine ecosystem. Photo-autotrophic organisms, mainly phytoplankton and macro-algae, fix this gas through photosynthesis in the euphotic zone and, in turn, produce organic matter and dissolved oxygen. Heterotrophic organisms, mainly heterotrophic protists and metazoans

https://doi.org/10.5194/gmd-2020-41
Preprint. Discussion started: 18 May 2020

Geoscientific Model Development Discussions

consume organic matter and dissolved oxygen by aerobic respiration and, in turn, produce CO_2. In the ocean, the main processes regulating CO_2 exchanges between the atmosphere and sea are the physical ones, also called the solubility pump and the biological pump. Overall, the thermohaline gradients drive the solubility pump, while the metabolic processes of gross primary production and respiration set the intensity of the biological pump (Raven and Falkowski, 1999).

The coastal zones, despite their small surface area and volume compared to those of the open ocean, have a large influence upon carbon dynamics and represent 14 to 30% of the oceanic primary production (Gattuso et al., 1998). At the interface between open-ocean and continents, these zones receive large inputs of nutrients and organic matters from rivers, groundwater discharge, and from atmospheric depositions (Cloern et al., 2014; Gattuso et al., 1998). On the coastline, coastal areas are subject to an increasing density of population and associated urbanization (Small and Nicholls, 2003). This rapid alteration of the coastline all over the world accelerates the emissions of greenhouses gases near the coastal ocean, and it also involves large discharges of material into the seawater by wastewater runoff and/or rivers (Cloern, 2001). These anthropogenic forcings alter the biogeochemical functioning of these zones and could lead to a growing eutrophication (Cloern, 2001). Moreover, these forcings could affect the carbonate chemistry dynamic and amplify the acidification in coastal zones. This alteration of the marine environment may provoke further changes in the structure of the plankton community, including *in fine* consequences on the populations with high trophic levels, such as teleosts (Esbaugh et al., 2012). At a global scale, coastal zones are considered to be a significant sink for atmospheric CO_2, with an estimated flux converging to 0.2 PgC y^{-1} (Roobaert et al., 2019). However, some studies highlight that the status of these areas as a sink or source still remains uncertain due to the complexity of the interactions between biological and physical processes, and also due to the lack of *in situ* measurements (Borges and Abril, 2011; Chen et al., 2013; Chen and Borges, 2009). Moreover, the capacity for coastal zones to absorb atmospheric CO_2 resulting from the increasing human pressure also remains poorly known. There are few works which highlight, under future atmospheric CO_2 levels, that shallow seas will become a net sink or a reduced source of CO_2 (Andersson and MacKenzie, 2012; Cai, 2011).

The current increase in CO_2 partial pressure (pCO_2) in the surface ocean is slowly shifting the marine carbonate chemistry equilibrium towards increases in pCO_2 and HCO_3^- and decreases in pH and CO_3^{2-} (Hoegh-Guldberg et al., 2018). These trends have already been described in several coastal and open-ocean locations worldwide (Cai et al., 2011). In a coastal Northwestern Mediterranean site, a 10-year time-series of *in situ* measurements highlights a trend of pH decrease and pCO_2 increase (Kapsenberg et al., 2017). Low pH values can inhibit the ability of many marine organisms to form the calcium carbonate ($CaCO_3$) used in the making of skeletons and shells (Gattuso et al., 2015). In an extreme case, this shift may promote dissolution of $CaCO_3$ because the water will become under-saturated with respect to $CaCO_3$ minerals (Doney et al., 2009).

The present study is dedicated to the assessment of the marine carbonate system variability in relation to physical and biogeochemical processes (gross primary production (GPP) and respiration (R)) in the Bay of Marseille (BoM), located in the Northwestern Mediterranean Sea (France). The BoM is subject to high emissions of atmospheric CO_2 from the nearby urban area, and also receives effluents from the Aix-Marseille metropolis. In addition, strong winds events regularly occur, which could lead to upwelling on the coast and to Rhone River plume intrusion under specific wind conditions (Fraysse et al., 2013, 2014). In this regional context, many anthropogenic forcings can interact with the dynamics of the carbonate systems. Natural determinants of the composition of the marine planktonic community can also play a crucial role in these dynamics.

Recently, Wimart-Rousseau et al. (2020) made a first assessment of the carbonate system dynamics of the BoM based on carbonate variable data recorded bimonthly at SOLEMIO station (Fig. 1C). Their work highlights that, on

https://doi.org/10.5194/gmd-2020-41
Preprint. Discussion started: 18 May 2020

Geoscientific Model Development Discussions

annual scale, the BoM acts as a sink of atmospheric CO_2, and that the temperature is the main driver of seawater pCO_2 variability on a yearly scale. In order to complete and improve our understanding of the carbonate system dynamics of the BoM at a higher temporal scale, a biogeochemical model is used. Modeling is a useful tool for deciphering the role of each of the aforementioned determinants in the dynamics of carbonate equilibrium. In the present study, a carbonate chemistry balance module has been developed and implemented within a biogeochemical model of the planktonic food web, namely Eco3M-CarbOx. The carbonate module has been evaluated against the *in situ* data obtained for the year 2017. Finally, this model is used to assess the variability of carbonate equilibrium and air-sea CO_2 fluxes, and to quantify the contribution of certain physical processes (e.g., wind events, river intrusions, temperature increases, and changes in atmospheric pCO_2 levels) to the variability of this equilibrium.

2. Materials & Methods

2.1 Study area

The BoM is located in the eastern part of the Gulf of Lions, in the Northwestern Mediterranean Sea (Fig. 1). The city of Marseille, located on the coast of the BoM, is the second largest city of France, with a population of *ca*. 1 million inhabitants. The Rhone River, which flows into the Gulf of Lions, is the greatest source of freshwater and nutrients for the Mediterranean Sea, with a river mean flow of 1800 m^3 s^{-1} (Pont et al., 2002). Several studies highlight the eastward intrusion events from the Rhone River plume in the BoM under East and South-easterly winds conditions, which favor biological productivity (Fraysse et al., 2014; Gatti et al., 2006; Para et al., 2010). The biogeochemistry of the BoM is complex and highly driven by hydrodynamics. North-north-westerly winds induce upwelling events which bring upward cold and nutrient-rich waters (Fraysse et al., 2013). Moreover, the oligotrophic Northern Current occasionally intrudes in the BoM (Petrenko, 2003; Ross et al., 2016).

Despite the presence of several marine protected areas around the BoM (the Regional Park of Camargue, the Marine protected area Côte Bleue and the National Park of Calanques), it is strongly impacted by diverse anthropogenic forcing, because industrialized and urbanized areas are located all along the coast. From the land, the BoM receives nutrients and organic matter from the urban area of the Aix-Marseille metropolis (Millet et al., 2018), the industrialized area of Fos-sur-Mer city (one of the biggest oil-based industry areas in Europe), and the Berre Lagoon, which is eutrophized (Gouze et al., 2008; Fig. 1C). From the atmosphere, the BoM is subject to fine particles deposition and greenhouse gas emissions (including CO_2) from the nearby urban area, and it also receives effluents from the Aix-Marseille metropolis.

2.2 Numerical model description

The Eco3M-CarbOx biogeochemical model has been developed to represent the dynamics of the seawater carbonate system and plankton food web in the BoM. The model was implemented using the Eco3M (Ecological Mechanistic and Modular Modelling) modeling platform (Baklouti et al., 2006). The model structure used is based on an existing model of the plankton ecosystem (Fraysse et al., 2013), including a description of C, N and P biogeochemical cycles. The Eco3M-CarbOx model includes 22 prognostic state variables that are split into 5 compartments: phytoplankton, heterotrophic bacteria, detritus, dissolved organic matter, nutrients (ammonia, nitrate and phosphate), dissolved oxygen, and carbonate system variables (Fig. 2). For this study, the phytoplankton is divided in two groups: one with traits of the *Synechococcus* cyanobacteria, which is one of the major constitutive members of pico-autotrophs in Mediterranean Sea (Mella-Flores et al., 2011), and another with traits of large diatoms, which are generally observed during spring blooms at mid-latitudes (Margalef, 1978). For both of the phytoplankton, there is a diagnostic

https://doi.org/10.5194/gmd-2020-41
Preprint. Discussion started: 18 May 2020

Geoscientific Model Development Discussions

chlorophyll-a variable related to the phytoplankton biomass in carbon, the phytoplankton N-to-C ratio, and the limiting internal ratio f_Q^N (Faure et al., 2010; Smith and Tett, 2000; Tab. A2).

Additionally, three state variables have been added in order to represent the carbonate dynamics: dissolved inorganic carbon (DIC), total alkalinity (TA) and the calcium carbonate ($CaCO_3$) implicitly representing calcifying organisms. The knowledge of DIC and TA allows the calculation of the pCO_2 and pH diagnostic variables, necessary for resolving all the equations of the carbonate system. These equations use apparent equilibrium constants, which depend on temperature, pressure, and salinity (Dickson, 1990a, 1990b; Dickson and Riley, 1979; Lueker et al., 2000; Millero, 1995; Morris and Riley, 1966; Mucci, 1983; Riley, 1965; Riley and Tongudai, 1967; Uppström, 1974; Weiss, 1974). Based on the review of Middelburg (2019), it is considered that: (i) TA decreases by 2 moles during the calcification and nitrification processes and by 1 mole when phytoplankton assimilates ammonium, and TA increases by 2 moles during the $CaCO_3$ dissolution, by 1 mole when phytoplankton assimilates nitrate and phosphate, and by 1 mole when bacteria mineralized organic matter in ammonium (See Appendix Tab. A2). (ii) DIC is consumed during the photosynthesis and calcification processes and is produced by respiration (of phytoplankton, zooplankton, and bacteria) and the $CaCO_3$ dissolution processes. Moreover, the dynamics of DIC are altered by CO_2 exchanges with the atmosphere (See Appendix Tab. A2). The air-sea CO_2 fluxes are calculated from the pCO_2 gradient across the air-sea interface and the gas transfer velocity estimated from wind speed and using the parametrization of Wanninkhof (1992).

In the Eco3M-CarbOx model, zooplankton is considered as an implicit variable. However, a closure term based on the assumption that all of the matter grazed by the zooplankton and higher trophic levels returns as either organic or inorganic matter by excretion, egestion and mortality processes is taken into account (Fraysse et al., 2013). The model considers a "non-redfieldian" stoichiometry for phytoplankton and bacteria. A summary of the biogeochemical model equations and parameters values is included in the Appendix.

2.3 Use data set

The modelled variables of the carbonate system (DIC, TA, *p*H and pCO_2) and chlorophyll-a are hereafter compared to observations collected at the SOLEMIO station (Figs. 1C & 3), which is a component of the French national monitoring network (Service d'Observation en Milieu Littoral - SOMLIT, http://somlit.epoc.u-bordeaux1.fr/fr/). Major biogeochemical parameters have been recorded since 1994. However, carbonate chemistry variables (pH, pCO_2, DIC and TA) have been available since 2016, every two weeks. To compare model with observations, we calculate the average modeled value of each variable at ±5 days around the sampling date.

2.4 Design of numerical experiments

In the present work, the Eco3M-CarbOx model was run for the whole year of 2017. This year has been chosen because *in situ* data of carbonate systems (DIC, TA, pH and pCO_2) are available for the whole year at the SOLEMIO station (Fig. 1C). The biogeochemical variables were initialized using *in situ* data from winter conditions (see Appendix Tab.A1). The model was forced by time-series of sea surface temperature and salinity, wind (at 10 m), light, and atmospheric CO_2 concentrations. The sea temperature time-series is from *in situ* hourly data recorded at the Planier station (Fig. 1C). For salinity, hourly *in situ* data from the SOLEMIO station and from the CARRY buoy were used (Fig. 1C). Wind and light hourly time-series were extracted from the WRF meteorological model at the SOLEMIO station (Yohia, 2017). Finally, we used hourly atmospheric CO_2 values from *in situ* measurements recorded at the *Cinq Avenues* station (CAV station, Fig. 1B) by the AtmoSud Regional Atmospheric Survey

https://doi.org/10.5194/gmd-2020-41
Preprint. Discussion started: 18 May 2020

Network, France (https://www.atmosud.org). This simulation is the reference simulation (noted S0). As highlighted previously, upwelling events and river plume intrusions (due to winds specific conditions) have an impact on the dynamics of primary production (Fraysse et al., 2014; Ross et al., 2016) and then on the seawater CO_2 concentrations. Moreover, the temperature and atmospheric CO_2 variations control the seawater CO_2 dynamics *via* the solubility equilibrium and gas exchange with the atmosphere (Middelburg, 2019). In order to quantify the impact of different forcings, several simulations (hereafter noted S), which are summarized in Table 1, were conducted:

- Impact of temperature increase, S1: the time-series was shifted by +1.5°C (Cocco et al., 2013).
- Impact of wind events: a first simulation S2 was run with a constant wind intensity of 7 m s^{-1} throughout the year and a second one (S3) with two three-day periods of strong wind speed (20 m s^{-1}) starting on May 15th and August 15th, and a constant value of 7 m s^{-1} the rest of the year.
- Impact of Rhone River plume intrusion (a salinity threshold of 37 has been chosen to identify the presence of low-salinity waters from the Rhone River plume):
  - Nitrate inputs were simulated during the river plume intrusions (S4): the level of nitrate supplied by the river depends on the salinity level. A relationship was established using NO_3 and salinity data at the SOLEMIO point from the MARS3D-RHOMA coupled physical and biogeochemical model (Fraysse et al., 2013; Pairaud et al., 2011), which has already been used to reproduce realistic observed conditions in the studies of Fraysse et al. (2014) and Ross et al. (2016): $NO_{3intrusion}$ (mmol m^{-3}) = -1.7×S + 65.
  - TA inputs were simulated during river plume intrusions (S5): the level of TA supply by the river depends on the salinity. A relationship was established using *in situ* data from the SOLEMIO station during river intrusion: $TA_{intrusion}$ (µmol kg^{-1}) = -21.0×S + 3400.
- Non-urban atmospheric CO_2 concentrations (S6): this simulation takes into account the forcing of atmospheric CO_2 values measured at the *Observatoire de Haute Provence* station (OHP, Fig. 1B) located outside of the Aix-Marseille metropolis from the ICOS National Network, France (http://www.obs-hp.fr/ICOS/Plaquette-ICOS-201407_lite.pdf).

In this work, we calculated the daily mean values of state variables, the statistical parameters and mean fluxes of modeled processes throughout the year and over two main hydrological periods: the stratified and mixed water column periods. The stratified water column (SWC) is defined with a temperature difference between the surface and bottom of more than 0.5°C (Monterey and Levitus, 1997). For the simulated year (2017), the SWC period lasts from May 10th to October 20th. The mixed water column (MWC) period corresponds to the rest of the year.

3. Results

3.1 Model skills

Following the recommendations of Rykiel (1996), three criteria have been considered to evaluate the performance of our model:

- Does the model reproduce the timing of the observed variations of carbonate system at the seasonal time scale?
- Does the model reproduce the observed pCO_2 and pH ranges at the seasonal time scale?
- Analysis of the Willmott Skill Score (WSS): this index is an objective measurement of the degree of agreement between the modeled results and the observed data. A correct representation of observations by the model is achieved when this index is higher than 0.70 (Willmott, 1982).

https://doi.org/10.5194/gmd-2020-41
Preprint. Discussion started: 18 May 2020

Over most of the studied period, the model simulates lower chlorophyll-a concentrations than the *in situ* observations, especially during the MWC period (Fig. 3A). Two maxima of chlorophyll-a concentrations are observed *in situ:* the first one at *ca*. 1.71 mg m^{-3} in March and the second one at *ca*. 0.68 mg m^{-3} in May. They are both linked to Rhone River plume intrusions. Several *in situ* maxima between 0.5 and 0.7 mg m^{-3} are observed between March and April (at the end of the MWC period), and they signaled the spring bloom event (Tab. 2 & Fig. 3A). The biogeochemical model quantitatively reproduces the spring bloom observed at the end of the MWC period (Fig. 3A) with a maximum value of *ca.* 0.69 mg m^{-3}. The model does not catch the two aforementioned maxima of chlorophyll, and it contains a low value of WSS and a strong bias (0.37 and +0.22 mg m^{-3}, respectively - Tab. 2).

On the whole, the seasonal variations of the seawater pCO_2 are correctly simulated by the biogeochemical model (Fig. 3B). The model especially succeeds in reproducing the observed increase in relation to high temperatures during the SWC period. The reduction of the CO_2 solubility due to thermal effects mostly explains the increase in pCO_2 during the SWC period. The strong standard deviation of modeled values during the SWC period can be explained by the rapid changes in temperature due to upwelling occurring at this time of the year. The range of modeled pCO_2 values (345 - 503 µatm) encompasses the range of observation values (358 - 471 µatm; Tab. 2). The model tends to slightly overestimate the pCO_2 values with a mean bias of +23 µatm, whereas statistical analysis calculates a WSS value of 0.69 (Tab. 2).

The seasonal dynamics of *p*H is mostly reproduced by the model, and in particular, the decrease during the SWC period (Fig. 3D). However, the modelled *p*H is generally underestimated throughout the year, except during the SWC period, with a mean bias of -0.015 (Tab. 2). The seasonal range is captured by the model with a minimum value during the SWC period (7.994 *vs.* 8.014 for observations; Tab.2) and a maximum one during the MWC period (8.137 *vs.* 8.114 for observations; Tab.2). The statistical analysis highlights an index of agreement between the *in situ* data and the model outputs higher than 0.70 (Tab. 2).

The seasonal variations of DIC show the highest values during the MWC period and a decrease (resp. increase) during the beginning (resp. the end) of the SWC period (Fig. 3D). The lowest values are observed during September. The Eco3M-CarbOx model closely matches the seasonal dynamic by reproducing the range of extreme observed values (Tab. 2). The mean bias is also small (-8.48 µmol kg^{-1}, Tab. 2). More than 70% (0.73, Tab. 2) of modeled DIC concentrations are in statistical agreement with the corresponding observations.

The seasonal cycle of measured TA does not show a clear pattern (Fig. 3F). Large variations of values ranging between 2561 and 2624 µmol kg^{-1} (Tab. 2) are observed, whatever the hydrological season is that is considered. The biogeochemical model provides almost constant values around 2570 µmol kg^{-1} all along the year. With a low WSS index of agreement and a large mean bias (Tab. 2), the model is not able to confidently reproduce the observed variations of TA (Fig. 3F & Tab. 2). However, it can be noted that the modeled values remain within the range of *in situ* data (Tab. 2).

3.2 Carbon fluxes and budgets

For the year 2017, the values of temperature vary between 13.3°C and 25.9°C (Fig. 4A). The DIC variations closely match those of temperature (correlation coef. -0.75). For example, the spring increase of temperature leads to a decrease in DIC concentrations (Figs. 4A & 4C), and the minimum values are reached at the end of SWC period. Over the simulated period, the air-sea CO_2 fluxes (F_{aera}) vary between -14 and 17 mmol m^{-3} d^{-1}, with a weakly positive annual budget of +6 mmol m^{-3} y^{-1} (or +0.017 mmol m^{-3} d^{-1}, Tab. 3). Then, the BoM waters would act as a net source of CO_2 to the atmosphere on an annual basis. However, on a seasonal basis, the BoM waters would change from a net sink during the MWC period (F_{aera} <0; Tab. 3) to a net source during the SWC one (F_{aera} >0; Tab. 3).

https://doi.org/10.5194/gmd-2020-41
Preprint. Discussion started: 18 May 2020

On an annual basis, the gross primary production (GPP) and total respiration (R) are balanced, leading to a null average net ecosystem production (NEP, NEP=GPP-R) (Fig. 4F & Tab. 3). The intensity of autotroph respiration (R_a) is lower than that of primary production (annual mean of 0.065 *vs.* -0.413 mmol m^{-3} d^{-1}, respectively - Tab. 3). While the zooplankton and bacterial respiration account for an average of 0.348 mmol m^{-3} d^{-1} (Tab. 3). On a seasonal basis, the model highlights an ecosystem dominated by autotrophy during the MWC period (NEP>0; Tab. 3) and heterotrophy during the SWC period with higher fluxes values (NEP<0; Tab. 3). The biogeochemical fluxes show the strongest variations along the SWC period, following those of temperature (Fig. 4F). The maximum GPP occurs in April and is correlated with the maximum chlorophyll concentration. At this time, the ecosystem is autotroph (NEP>0; Figs. 4B & 4F), and is a net sink for atmospheric CO_2, which explains the DIC and seawater pCO_2 decreases during the bloom period (Figs. 4C, 4D & 4E)

When looking in-detail at the temperature and salinity 2017 time-series (Fig. 4A), several crucial events can be seen occurring, including freshwater intrusions (*e.g.* 15 March and 6 May) into the BoM and large variations of temperature in relation with upwelling events. The largest freshwater intrusion from the Rhone River plume occurs in mid-March, with a minimum observed salinity of *ca.* 32.5 at the SOLEMIO station (Fig. 4A). During this event, the seawater pCO_2 decreases and *p*H increases concomitantly (Figs. 4C & 4D). Then, seawater appears to be temporarily under-saturated in CO_2 and the BoM waters thus acts as a sink for atmospheric CO_2 at the time of intrusion (Fig. 4E).

During the SWC period, upwelling events quickly cool the surface seawater. In two days, from July 25th to 27th, the water temperature drops from 24.7°C to 16.9°C (Fig. 4G). The decrease in temperature corresponds with the increase in DIC concentrations (Fig. 4I). Concomitantly, the values of seawater pCO_2 decrease from 497 to 352 µatm and *p*H increase from 7.99 to 8.12 (Figs. 4I & 4J). This event quickly changes the BoM waters from a source to a sink for atmospheric CO_2 (from +17 to -14 mmol m^{-3} d^{-1}, Fig. 4K), and also from a net heterotroph to a net autotroph ecosystem (Fig. 4L).

3.3 Impact of external forcing on the dynamics of carbonate system

3.3.1 Temperature increase

Here we compare the reference simulation S0 with the S1 simulation (seawater temperature elevation of 1.5°C - Fig. 5). During the year, there are few changes on the carbonate system variables such as the pCO_2 and *p*H (data not shown). The main alterations occur during the blooms of phytoplankton. The simulated bloom of phytoplankton occurs later, at beginning of May, for both diatoms and picophytoplankton, with a maximum value of chlorophyll of 1.4 and 0.4 mg m^{-3}, respectively (Figs. 5A & 5F).

As both the limitations due to light and nutrients remain about the same during the simulations S0 and S1, this counterintuitive occurrence of bloom relative to changes in temperature is mainly explained by the temperature limiting function, which depends on the optimal temperature of growth (T_{opt}). For the picophytoplankton, from January to April, the increase of 1.5°C drastically reduces the limitation by temperature (Fig. 5C), because the temperature is closer to the optimal temperature (T_{opt}=16°C, Tab. A4) during S1 than S0. In the S0 simulation, the temperature reaches T_{opt} *ca.* April 15th and it induces the bloom, while at the same time in S1 the temperature moves slightly away from T_{opt} and it does not enable the triggering of a bloom. At the time of the bloom in S1, the opposite configuration occurs. In S0, the ambient temperature is again far from T_{opt}, explaining the absence of bloom, while in the S1 the ambient temperature is closer to T_{opt} enabling the occurrence of bloom. The picophytoplankton bloom then occurs later in the warm simulation S1 than in the reference simulation S0 (Fig. 5A). The duration and termination of bloom is controlled both by the nutrients availability and the temperature (Figs. 5C & 5D). Inversely,

https://doi.org/10.5194/gmd-2020-41
Preprint. Discussion started: 18 May 2020


Geoscientific Model Development Discussions

from January to April, the diatoms growth limitation by temperature is strengthened in the warm simulation S1 (Fig. 5H), because the resulting ambient temperature is farer from the optimum temperature (T_{opt}=13°C, Tab. A4) than that in the reference simulation S0. This induces a slower growth of diatoms and a delay of the maximum concentration (Fig. 5F). Afterwards the photosynthesis is mainly limited by temperature (Fig. 5H).

The ecosystem is net autotroph at the time of blooms whatever the simulation considered (NEP>0; Fig. 5E) and the quantity of DIC (not shown) fixed through autotroph processes is larger than that released by heterotroph processes. During the short period of bloom, the seawater pCO_2 decreases, leading to some negative air-sea fluxes (*i.e.* an oceanic sink for atmospheric CO_2). In the warm simulation, the later occurrence of bloom enables the period of the spring sink to extend by *ca*. three weeks over May relative to the reference simulation (Fig. 5J).

3.3.2 Wind speed

The Bay of Marseille is periodically under the influence of strong wind events (Millot, 1990). Here we compare two simulations: one with a constant wind value (S2) and the other one with two wind events that occur in May and August (S3) (Figs. 6A & D). The result of this numerical experiment shows that the stronger the wind speed is, the higher the air-sea fluxes are, mainly owing to the increase in gas transfer velocity. Depending on the gradient of CO_2 between seawater and the atmosphere, strong wind speeds will favor either the in-gassing or outgassing of CO_2 (Figs. 6B & E). In May, with the air-sea CO_2 flux being positive, the outgassing of CO_2 to the atmosphere is enhanced leading to a decrease in seawater pCO_2 (Fig. 6C). On the contrary, in August the oceanic sink of atmospheric CO_2 is amplified which leads to an increase in the seawater pCO_2 value (Fig. 6F).

3.3.3 Supply in nitrate and alkalinity by river inputs

According to the model results (Fig. 7), the occasional inputs of nitrate (S4) that are linked to river plume intrusions favor primary production and they led to increased chlorophyll concentrations (Figs. 7B & 7C) five times during the SWC period. These blooms, as seen previously, lead to a decrease (resp. increase) in the seawater pCO_2 (resp. *p*H) (Figs. 7E & 7F). It can be noted that the strongest river supply at mid-March (Figs. 7A & 7B) does not involve a bloom immediately, but it may favor the occurrence of the spring bloom earlier (Fig. 7C) than that of the reference simulation (S0). The time lag between river nutrient supply and bloom is due to the temperature limitation (Fig. 4C). During blooms occurring within the SWC period following intrusions, the DIC concentrations are generally lower than those of the reference simulation, as in the case of the bloom of mid-May (decrease by *ca*. 15 µmol kg^{-1}, Fig. 7J), due to the autotroph processes dominating the heterotroph ones. In turn, the seawater pCO_2 drops by *ca*. 30 µatm (Fig. 7K) and *p*H increases by *ca*. 0.030 (Fig. 7L). Nitrate inputs, favoring primary production, reduce the source of CO_2 to the atmosphere or intensify the sink of atmospheric CO_2 into the waters of BoM (Fig. 7E & 7K).

The supply of alkalinity during the Rhone River plume intrusions (Fig. 8A) significantly increases the DIC concentrations (*ca*. +50 µmol kg^{-1}, Figs. 8B & 8F), in every hydrological period considered. During the strongest freshwater input at mid-March, the sharp TA increase by *ca*. +150 µmol kg^{-1} (Fig. 8E) leads to a large pCO_2 drop by *ca*. 92 µatm and a *p*H increase by 0.13 (Figs. 8G & 8H). The air-sea gradient of pCO_2 increases at mid-March, favoring sink conditions for atmospheric CO_2 into the waters of the BoM (Fig. 8G)

3.3.4 Urban air CO_2 concentrations

The Aix-Marseille metropolis is strongly subject to urban emissions to the atmosphere (Xueref-Remy et al., 2018a). The variability of atmospheric CO_2 concentrations at the urban site (CAV station, Fig. 1) is much higher than that observed in a non-urban area (OHP station, Fig. 1), especially during the MWC period (Fig. 9A): CO_2 concentrations

https://doi.org/10.5194/gmd-2020-41
Preprint. Discussion started: 18 May 2020


Geoscientific Model Development Discussions

vary between 379 and 547 µatm at the CAV station and between 381 and 429 µatm at the OHP station. Moreover, in winter the atmospheric pCO_2 is higher in the urban area than non-urban area, whereas in summer those of both areas are quite close. These differences in the seasonal pattern and between areas are usually explained by (i) the thinner atmospheric boundary layer, (ii) the decreased fixation of CO_2 by terrestrial vegetation, and (iii) the greater influence of anthropogenic activities by emissions from heating (Xueref-Remy et al., 2018b). Forcing the model by atmospheric pCO_2 values from urban or non-urban site can lead to significant differences in the values of the seawater pCO_2 during the MWC period especially. The air-sea gradient of pCO_2 is higher when using a forcing derived from the CO_2 concentrations originating from an urban area than from non-urban area, which strengthens the sink of atmospheric CO_2 into the waters of BoM. The seawater pCO_2 is then lower with non-urban area pressure (S6) than with urban area pressure (S0), because of weaker CO_2 solubility in the BoM (Fig. 9B).

4. Discussion

4.1 Model performance

The evaluation of model skill *vs. in situ* data highlights that the modeled *p*H, pCO_2, DIC are in acceptable agreement with observations (Fig. 3). The seasonal variations observed for the different variables are captured by the model, including for example the seasonal decrease in DIC and *p*H during the SWC period, in relation to the increase in pCO_2, and the inverse scenario during the MWC period. The chlorophyll content variability is not well reproduced, especially during spring (Fig. 3A), even taking into account the nitrate supply from the Rhone River plume intrusion (Fig. 7C). This is due to the multiple origins of chlorophyll, organic matter, and nutrients in the BoM that are not accounted for in the Eco3M-CarbOx model: autochthonous marine production, and allochthonous origins from the Rhone and Huveaune River plumes (Fraysse et al., 2013). The observed variations and levels of TA are not correctly simulated by the model (Fig. 3F), even taking into account the supply of TA coming from the Rhone River plume (Fig. 8). The formulation used in this study for TA inputs from rivers needs to be refined and compared with other works (Gemayel et al., 2015; Schneider et al., 2007). The study of Soetaert et al. (2007) highlights that the main variations of TA in the marine coastal zones are linked to freshwater supplies and marine sediments. The present study does not take into account the inputs of TA from the water-sediment interface, and it may explain why the TA variable is not correctly predicted by our model.

4.2 Contribution of physical and biogeochemical processes to the variability of carbonate system

The contribution of each biogeochemical process to the DIC variability can be assessed using the presented model: the aeration process contributes to 78% of the DIC variations and biogeochemical processes together to 22% (Tab. 3). As mentioned by Wimart-Rousseau et al. (2020), the model suggests that the seawater pCO_2 variations and associated fluxes would be mostly driven by the seawater temperature dynamics. Moreover, the seasonal variations of the air-sea CO_2 flux are in agreement with some previous *field* studies (De Carlo et al., 2013; Wimart-Rousseau et al., 2020), which measured a weak oceanic sink for atmospheric CO_2 during winter and a weak source to the atmosphere during summer.

The model results reveal that temperature would play a crucial role in controlling two counterbalanced processes: (1) the carbonate system equilibrium and (2) the phytoplankton growth. The increase in temperature during SWC leads to a higher pCO_2 in seawater due to the decrease in the CO_2 solubility (Middelburg, 2019) and, at the same time, the fixation of DIC by phytoplankton is favored, leading to a decrease in the pCO_2 level. The imbalance between the latter two processes leads to a change in the ecosystem status (autotrophic or heterotrophic) and the corresponding

https://doi.org/10.5194/gmd-2020-41
Preprint. Discussion started: 18 May 2020

behavior as a sink or source to the atmosphere. In case of a 1.5°C rise over the whole year, the temperature variation has a very small impact on the carbonate system dynamics. However, it favors the autotrophic processes and strengthens the oceanic sink of atmospheric CO_2 during the bloom of phytoplankton (Figs. 5E & 5J).

4.3 Contribution of the external forcings to the variability of carbonate system

In line with several previous works on the Northwestern Mediterranean Sea (De Carlo et al., 2013; Copin-Montégut et al., 2004)(De Carlo et al., 2013; Copin-Montégut et al., 2004; Wimart-Rousseau et al., 2020), the model also suggests that the status of the Bay of Marseille regarding sink or source for CO_2 could change at high temporal frequency (*i.e.* hours to days). Upwelling events that are the consequence of North, Northwestern winds, lead to a decrease in seawater temperature (<2 days, Fig. 4G), involving a decrease in the seawater pCO_2 values (Fig. 4J) and *in fine*, an alteration of the CO_2 air-sea fluxes. Model results suggest that the fast variations of temperature could lead to rapid changes of the sink *vs.* source status in this coastal zone (Fig. 4K). Moreover, previous study on the BoM highlights that upwelling favors ephemeral blooms of phytoplankton by nutrient supplies up to euphotic layer (Fraysse et al., 2013) and would, in turn, contribute to the seawater pCO_2 decrease. Upwelling events could then enhance the sink for atmospheric CO_2 due to the temperature drop and nutrients inputs. High wind speeds (>7 m s^{-1}) amplified considerably the gaseous exchange of CO_2 (De Carlo et al., 2013; Copin-Montégut et al., 2004; Wimart-Rousseau et al., 2020). The model highlights that a strong wind event of 3 days has a significant impact on the seawater pCO_2 values during a longer period *ca.* 15 days (Fig. 6). A combination of high atmospheric pCO_2 value and wind speed would then favor the sink for CO_2 into the waters of the BoM. The aeration process depends also on the choice of the formulation of the gas transfer velocity (k_{600}). In this study, the formulation of Wanninkhof (1992) is used and depends of the wind speed at 10 m above the water surface. However, the current velocity could favor the gas exchange and suspended matter concentration could limit the gas exchange (Abril et al., 2009; Upstill-Goddard, 2006; Zappa et al., 2003). Due to the important heterogeneity of physical and biogeochemical forcings in coastal zones, other factors that control the air-sea gas exchange should certainly be taken into account.

The simulation with intrusions of the Rhone River plume shows that inputs of nitrate and TA cause a drop of seawater pCO_2 due to some two concomitant effects: nutrients supply favors the phytoplankton development and TA inputs shift the carbonate system equilibrium leading to a pCO_2 decrease and DIC increase (Middelburg, 2019) (Figs. 7 & 8). The consequence is that the oceanic sink of CO_2 is enhanced. The intrusions of Rhone River plume induce a salinity decrease in the BoM waters, which leads to drop the pCO_2 levels. The drop of pCO_2 is due to the decrease in CO_2 solubility when salinity decreases (Middelburg, 2019).

In the scenario of forcing the model by using urban atmospheric pCO_2 time-series, the air-sea gradient increases and then, it enhances the status of the BoM as a sink for atmospheric CO_2. As suggested by the *in situ* study of Wimart-Rousseau et al. (2020), the Eco3M-Carbox model highlights the crucial role of the coastal ocean in urbanized area, with an increase in atmospheric CO_2, the CO_2 in-gassing by the costal ocean may increase. This results is in line with studies of Andersson and Mackenzie (2004) and Cai (2011) that predict an increase in the intensity of CO_2 sink in coastal areas due to high atmospheric CO_2 levels and a potential threat to coastal marine biodiversity.

5. Conclusion

The carbonate chemistry module has been implemented in the Eco3M-CarbOx biogeochemical model and compared against *in situ* data measured in the BoM. This evaluation shows that the model can be reasonably used to assess the

https://doi.org/10.5194/gmd-2020-41
Preprint. Discussion started: 18 May 2020


Geoscientific Model Development Discussions

sensitivity of carbon balance to physical processes (temperature and salinity), biogeochemical processes (GPP and respiration processes) and external forcing (wind, river intrusion and atmospheric CO_2).

The model results suggest that the carbonate system is mainly driven by the seawater temperature dynamics. At a seasonal scale, the BoM marine waters appear to be a net sink of atmospheric CO_2 and a dominant autotroph ecosystem during the MWC period, and a net source of CO_2 to the atmosphere during the SWC period, which is mainly characterized by a dominance of heterotroph processes. However, the model results highlight that upwelling events occurring within the SWC period quickly decrease the seawater temperature, which causes the CO_2 status of the BoM marine waters to change from a source to the atmosphere to a sink into the ocean within a few days. External forcing as the temperature increases leads to a delay in the bloom of phytoplankton. Strong wind events enhance the gas exchange of CO_2 with the atmosphere. A river plume intrusion with input of nitrate and alkalinity favors pCO_2 decreases, and the sink of atmospheric CO_2 into the BoM waters is enhanced. The higher air pCO_2 values from the urban area intensify the oceanic sink of atmospheric CO_2.

The BoM biogeochemical functioning is mainly forced by wind-driven hydrodynamics (upwelling and downwelling), urban rivers, wastewater treatment plants, and atmospheric deposition (Fraysse et al., 2013). In addition, Northern Current and Rhone River plume intrusions frequently occurred (Fraysse et al., 2014; Ross et al., 2016). Thus, a 3D coupled hydrodynamic and biogeochemical model will be urgently needed to mirror the complexity of the BoM functioning. In this way, the contributions of hydrodynamic, atmospheric, anthropic, and biogeochemical processes to the DIC variability could be determined, and an overview of the air-sea CO_2 exchange could be made at the scale of the Bay of Marseille. Moreover, in this paper we highlighted that fast and strong variations of pCO_2 values occur, so thus it is essential to acquire more *in situ* values at high frequency (at least with an hourly resolution) to understand the rapid variations of the marine carbon system at these short spatial and temporal scales.

https://doi.org/10.5194/gmd-2020-41
Preprint. Discussion started: 18 May 2020

Acknowledgements

We thank the National Service d'Observation en MILieu Littoral (SOMLIT) for its permission to use SOLEMIO data. We wish to thank the crewmembers of the R.V. 'Antedon II', operated by the DT-INSU, for making these samplings possible. We wish to acknowledge the team of the SAM platform (Service Atmosphère Mer) of MIO institute for their helping in field work. For the collection and analyses of the seawater sample, we thank Michel Lafont and Véronique Lagadec of the PACEM (Plateforme Analytique de Chimie des Environnenemnts Marins) platform of MIO institute and also the SNAPO-CO2 at LOCEAN, Paris. The SNAPO-CO2 service at LOCEAN is supported by CNRS-INSU and OSU Ecce-Terra.

We acknowledge the staff of the "Cluster de calcul intensif HPC" Platform of the OSU Institut Pythéas (Aix-Marseille Université, INSU-CNRS) for providing the computing facilities. We gratefully acknowledge Julien Lecubin from the Service Informatique de OSU Institut Pythéas (SIP) for their technical assistance. Moreover we thank Camille Mazoyer and Claire Seceh for their contribution on the Eco3M-CarbOx model development.

Financial support

This study takes part of the AMC project (Aix-Marseille Carbon Pilot Study, 2016-2019) funded and performed in the framework of the Labex OT-MED (ANR-11-LABEX-0061, part of the "Investissement d'Avenir" program through the A*MIDEX project ANR-11-IDEX-0001-02), funded by the French National Research Agence (ANR). The project leading to this publication has received funding from European FEDER Fund under project 1166-39417.

Code availability

Eco3M is freely available under CeCILL license agreement (a French equivalent to the L-GPL license; http://cecill.info/licences/Licence_CeCILL_V1.1-US.html; last access: 10 February 2020). The Eco3M-CarbOx model is written in Fortran-90/95 and the plotting code is written in Matlab®. The exact version of the model used to produce the results used in this paper is archived on Zenodo (DOI: 10.5281/zenodo.3757677) (last access: 20 April 2020).

https://doi.org/10.5194/gmd-2020-41
Preprint. Discussion started: 18 May 2020

Geoscientific Model Development Discussions

References

Abril, G., Commarieu, M. V., Sottolichio, A., Bretel, P. and Guérin, F.: Turbidity limits gas exchange in a large macrotidal estuary, Estuar. Coast. Shelf Sci., 83, 342–348, doi:10.1016/j.ecss.2009.03.006, 2009.

Allen, M. R., Frame, D. J., Huntingford, C., Jones, C., Lowe, J. A., Meinshausen, M. and Meinshausen, N.: Warming caused by cumulative carbon emissions towards the trillionth tonne, Nature, 458, 1163–1166, doi:10.1038/nature08019, 2009.

Andersson, A. J. and Mackenzie, F. T.: Shallow-water oceans: a source or sink of atmospheric CO_2?, Front. Ecol. Environ., 2(7), 348–353, doi:10.1890/1540-9295, 2004.

Andersson, A. J. and MacKenzie, F. T.: Revisiting four scientific debates in ocean acidification research, Biogeosciences, 9(3), 893–905, doi:10.5194/bg-9-893-2012, 2012.

Auger, P. A., Diaz, F., Ulses, C., Estournel, C., Neveux, J., Joux, F., Pujo-Pay, M. and Naudin, J. J.: Functioning of the planktonic ecosystem on the Gulf of Lions shelf (NW Mediterranean) during spring and its impact on the carbon deposition: a field data and 3-D modelling combined approach, Biogeosciences, 8(11), 3231–3261, doi:10.5194/bg-8-3231-2011, 2011.

Baklouti, M., Diaz, F., Pinazo, C., Faure, V. and Quéguiner, B.: Investigation of mechanistic formulations depicting phytoplankton dynamics for models of marine pelagic ecosystems and description of a new model, Prog. Oceanogr., 71(1), 1–33, doi:10.1016/j.pocean.2006.05.002, 2006.

Borges, A. V and Abril, G.: Carbon Dioxide and Methane Dynamics in Estuaries, in Treatise on Estuarine and Coastal Science, edited by E. Wolanski and D. McLusky, pp. 119–161, Academic Press, Waltham., 2011.

Le Borgne, R.: Zooplankton production in the eastern tropical Atlantic Ocean: Net growth efficiency and P:B in terms of carbon, nitrogen, and phosphorus, Limnol. Oceanogr., 27(4), 681–698, doi:10.4319/lo.1982.27.4.0681, 1982.

Le Borgne, R. and Rodier, M.: Net zooplankton and the biological pump: a comparison between the oligotrophic and mesotrophic equatorial Pacific, Deep Sea Res. Part II Top. Stud. Oceanogr., 44(9), 2003–2023, doi:10.1016/S0967-0645(97)00034-9, 1997.

Cai, W.-J.: Estuarine and Coastal Ocean Carbon Paradox: CO_2 Sinks or Sites of Terrestrial Carbon Incineration?, Ann. Rev. Mar. Sci., 3(1), 123–145, doi:10.1146/annurev-marine-120709-142723, 2011.

Cai, W.-J., Hu, X., Huang, W.-J., Murrell, M. C., Lehrter, J. C., Lohrenz, S. E., Chou, W.-C., Zhai, W., Hollibaugh, J. T., Wang, Y., Zhao, P., Guo, X., Gundersen, K., Dai, M. and Gong, G.-C.: Acidification of subsurface coastal waters enhanced by eutrophication, Nat. Geosci., 4(11), 766–770, doi:10.1038/ngeo1297, 2011.

Campbell, R., Diaz, F., Hu, Z., Doglioli, A., Petrenko, A. and Dekeyser, I.: Nutrients and plankton spatial distributions induced by a coastal eddy in the Gulf of Lion. Insights from a numerical model, Prog. Oceanogr., 109, 47–69, doi:10.1016/j.pocean.2012.09.005, 2013.

De Carlo, E. H., Mousseau, L., Passafiume, O., Drupp, P. S. and Gattuso, J.-P.: Carbonate Chemistry and Air–Sea CO_2 Flux in a NW Mediterranean Bay Over a Four-Year Period: 2007–2011, Aquat. Geochemistry, 19(5–6), 399–442, doi:10.1007/s10498-013-9217-4, 2013.

Chen, C.-T. A. and Borges, A. V: Deep-Sea Research II Reconciling opposing views on carbon cycling in the coastal ocean : Continental shelves as sinks and near-shore ecosystems as sources of atmospheric CO_2, Deep Sea Res. II, 56, 578–590, doi:10.1016/j.dsr2.2009.01.001, 2009.

Chen, C.-T. A., Huang, T.-H., Chen, Y.-C., Bai, Y., He, X. and Kang, Y.: Air–sea exchanges of CO_2 in the world's coastal seas, Biogeosciences, 10(10), 6509–6544, doi:10.5194/bg-10-6509-2013, 2013.

Cloern, J. E.: Our evolving conceptual model of the coastal eutrophication problem, Mar. Ecol. Prog. Ser., 210, 223–253, doi:10.3354/meps210223, 2001.

Cloern, J. E., Foster, S. Q. and Kleckner, A. E.: Phytoplankton primary production in the world's estuarine-coastal ecosystems, Biogeosciences, 11, 2477–2501, doi:10.5194/bg-11-2477-2014, 2014.

Cocco, V., Joos, F., Steinacher, M., Frölicher, T. L., Bopp, L., Dunne, J., Gehlen, M., Heinze, C., Orr, J., Oschlies, A., Schneider, B., Segschneider, J. and Tjiputra, J.: Oxygen and indicators of stress for marine life in multi-model global warming projections, Biogeosciences, 10(3), 1849–1868, doi:10.5194/bg-10-1849-2013, 2013.

Copin-Montégut, C., Bégovic, M. and Merlivat, L.: Variability of the partial pressure of CO_2 on diel to annual time scales in the Northwestern Mediterranean Sea, Mar. Chem., 85(3), 169–189, doi:10.1016/j.marchem.2003.10.005, 2004.

Dickson, A. G.: Standard potential of the reaction: AgCl(s) + $12H_2$ (g) = Ag(s) + HCl(aq), and and the standard acidity constant of the ion HSO4− in synthetic sea water from 273.15 to 318.15 K, J. Chem. Thermodyn., 22(2), 113–127, doi:10.1016/0021-9614(90)90074-Z, 1990a.

Dickson, A. G.: Thermodynamics of the dissociation of boric acid in synthetic seawater from 273.15 to 318.15 K, Deep Sea Res. Part A. Oceanogr. Res. Pap., 37(5), 755–766, doi:10.1016/0198-0149(90)90004-F, 1990b.

Dickson, A. G. and Riley, J. P.: The estimation of acid dissociation constants in sea-water media from potentiometric titrations with strong base. II. The dissociation of phosphoric acid, Mar. Chem., 7(2), 101–109, doi:10.1016/0304-4203(79)90002-1, 1979.

https://doi.org/10.5194/gmd-2020-41
Preprint. Discussion started: 18 May 2020

Doney, S. C., Tilbrook, B., Roy, S., Metzl, N., Le Quéré, C., Hood, M., Feely, R. a. and Bakker, D.: Surface-ocean CO_2 variability and vulnerability, Deep Sea Res. Part II Top. Stud. Oceanogr., 56(8–10), 504–511, doi:10.1016/j.dsr2.2008.12.016, 2009.

Esbaugh, A. J., Heuer, R. and Grosell, M.: Impacts of ocean acidification on respiratory gas exchange and acid--base balance in a marine teleost, Opsanus beta, J. Comp. Physiol. B, 182(7), 921–934, doi:10.1007/s00360-012-0668-5, 2012.

Faure, V., Pinazo, C., Torréton, J.-P. and Jacquet, S.: Modelling the spatial and temporal variability of the SW lagoon of New Caledonia I: A new biogeochemical model based on microbial loop recycling, Mar. Pollut. Bull., 61(7), 465–479, doi:10.1016/j.marpolbul.2010.06.041, 2010.

Fraysse, M., Pinazo, C., Faure, V., Fuchs, R., Lazzari, P., Raimbault, P. and Pairaud, I.: Development of a 3D Coupled Physical-Biogeochemical Model for the Marseille Coastal Area (NW Mediterranean Sea): What Complexity Is Required in the Coastal Zone?, PLoS One, 8(12), 1–18, doi:10.1371/journal.pone.0080012, 2013.

Fraysse, M., Pairaud, I., Ross, O. N., Faure, V. and Pinazo, C.: Intrusion of Rhone River diluted water into the Bay of Marseille: Generation processes and impacts on ecosystem functioning, J. Geophys. Res. Ocean., 119(10), 6535–6556, doi:10.1002/2014JC010022, 2014.

Fukuda, R., Ogawa, H., Nagata, T. and Koike, I.: Direct Determination of Carbon and Nitrogen Contents of Natural Bacterial Assemblages in Marine Environments, Appl. Environ. Microbiol., 64(9), 3352–3358 [online] Available from: https://aem.asm.org/content/64/9/3352, 1998.

Gatti, J., Petrenko, A., Devenon, J.-L., Leredde, Y. and Ulses, C.: The Rhone river dilution zone present in the northeastern shelf of the Gulf of Lion in December 2003, Cont. Shelf Res., 26(15), 1794–1805, doi:10.1016/j.csr.2006.05.012, 2006.

Gattuso, J.-P., Frankignoulle, M. and Wollast, R.: Carbon and carbonate metabolism in coastal aquatic ecosystems, Annu. Rev. Ecol. Syst., 29(1), 405–34, doi:10.1146/annurev.ecolsys.29.1.405, 1998.

Gattuso, J.-P., Magnan, A., Bille, R., Cheung, W. W. L., Howes, E. L., Joos, F., Allemand, D., Bopp, L., Cooley, S. R., Eakin, C. M., Hoegh-Guldberg, O., Kelly, R. P., Portner, H.-O., Rogers, A. D., Baxter, J. M., Laffoley, D., Osborn, D., Rankovic, A., Rochette, J., Sumaila, U. R., Treyer, S. and Turley, C.: Contrasting futures for ocean and society from different anthropogenic CO_2 emissions scenarios, Science, 349(6243), pp.aac4722, doi:10.1126/science.aac4722, 2015.

Gehlen, M., Gangstø, R., Schneider, B., Bopp, L., Aumont, O. and Ethe, C.: The fate of pelagic $CaCO_3$ production in a high CO_2 ocean: a model study, Biogeosciences, 4(4), 505–519, doi:10.5194/bg-4-505-2007, 2007.

Gemayel, E., Hassoun, A. E. R., Benallal, M. A., Goyet, C., Rivaro, P., Abboud-Abi Saab, M., Krasakopoulou, E., Touratier, F. and Ziveri, P.: Climatological variations of total alkalinity and total dissolved inorganic carbon in the Mediterranean Sea surface waters, Earth Syst. Dyn., 6(2), 789–800, doi:10.5194/esd-6-789-2015, 2015.

Gerber, R. P. and Gerber, M. B.: Ingestion of natural particulate organic matter and subsequent assimilation, respiration and growth by tropical lagoon zooplankton, Mar. Biol., 52(1), 33–43, doi:10.1007/BF00386855, 1979.

Gouze, E., Raimbault, P., Garcia, N. and Picon, P.: Nutrient dynamics and primary production in the eutrophic Berre Lagoon (Mediterranean , France), Transitional Waters Bull., 2, 17–40, doi:10.1285/i18252273v2n2p17, 2008.

Gruber, N., Clement, D., Carter, B. R., Feely, R. A., van Heuven, S., Hoppema, M., Ishii, M., Key, R. M., Kozyr, A., Lauvset, S. K., Lo Monaco, C., Mathis, J. T., Murata, A., Olsen, A., Perez, F. F., Sabine, C. L., Tanhua, T. and Wanninkhof, R. H.: The oceanic sink for anthropogenic CO_2 from 1994 to 2007, Science, 363(6432), 1193–1199, doi:10.1126/science.aau5153, 2019.

Gutiérrez-Rodríguez, A., Latasa, M., Scharek, R., Massana, R., Vila, G. and Gasol, J. M.: Growth and grazing rate dynamics of major phytoplankton groups in an oligotrophic coastal site, Estuar. Coast. Shelf Sci., 95(1), 77–87, doi:10.1016/j.ecss.2011.08.008, 2011.

Harrison, W. G., Harris, L. R. and Irwin, B. D.: The kinetics of nitrogen utilization in the oceanic mixed layer: Nitrate and ammonium interactions at nanomolar concentrations, Limnol. Oceanogr., 41(1), 16–32, doi:10.4319/lo.1996.41.1.0016, 1996.

Hoegh-Guldberg, O., Jacob, D., Taylor, M., Bindi, M., Brown, S., Camilloni, I., Diedhiou, A., Djalante, R., Ebi, K., Engelbrecht, F., Guiot, J., Hijioka, Y., Mehrotra, S., Payne, A., Seneviratne, S. I., Thomas, A., Warren, R. and Zhou, G.: Impacts of 1.5°C Global Warming on Natural and Human Systems, in Global warming of 1.5°C. An IPCC Special Report on the impacts of global warming of 1.5°C above pre-industrial levels and related global greenhouse gas emission pathways, in the context of strengthening the global response to the threat of climate change, edited by V. Masson-Delmotte, P. Zhai, H. O. Pörtner, D. Roberts, J. Skea, P. R. Shukla, A. Pirani, W. Moufouma-Okia, C. Péan, R. Pidcock, S. Connors, J. B. R. Matthews, Y. Chen, X. Zhou, M. I. Gomis, E. Lonnoy, T. Maycock, M. Tignor, and T. Waterfield, World Meteorological Organization Technical Document., 2018.

Kapsenberg, L., Alliouane, S., Gazeau, F., Mousseau, L. and Gattuso, J.-P.: Coastal ocean acidification and increasing total alkalinity in the northwestern Mediterranean Sea, Ocean Sci., 13(3), 411–426, doi:10.5194/os-13-411-2017, 2017.

Lacroix, G. and Grégoire, M.: Revisited ecosystem model (MODECOGeL) of the Ligurian Sea: seasonal and interannual variability due to atmospheric forcing, J. Mar. Syst., 37(4), 229–258, doi:10.1016/S0924-7963(02)00190-

https://doi.org/10.5194/gmd-2020-41
Preprint. Discussion started: 18 May 2020

2, 2002.

Leblanc, K., Quéguiner, B., Diaz, F., Cornet, V., Michel-Rodriguez, M., Durrieu de Madron, X., Bowler, C., Malviya, S., Thyssen, M., Grégori, G., Rembauville, M., Grosso, O., Poulain, J., de Vargas, C., Pujo-Pay, M. and Conan, P.: Nanoplanktonic diatoms are globally overlooked but play a role in spring blooms and carbon export, Nat. Commun., 9(1), 953, doi:10.1038/s41467-018-03376-9, 2018.

Lueker, T. J., Dickson, A. G. and Keeling, C. D.: Ocean pCO_2 calculated from dissolved inorganic carbon, alkalinity, and equations for K1 and K2: Validation based on laboratory measurements of CO_2 in gas and seawater at equilibrium, Mar. Chem., 70(June 2015), 105–119, doi:10.1016/S0304-4203(00)00022-0, 2000.

Margalef, R.: Life-forms of phytoplankton as survival alternatives in an unstable environment, edited by Gauthier-Villars, Oceanol. Acta, 1(4), 493–509 [online] Available from: https://archimer.ifremer.fr/doc/00123/23403/, 1978.

Marty, J.-C., Chiavérini, J., Pizay, M.-D. and Avril, B.: Seasonal and interannual dynamics of nutrients and phytoplankton pigments in the western Mediterranean Sea at the DYFAMED time-series station (1991–1999), Deep Sea Res. Part II Top. Stud. Oceanogr., 49(11), 1965–1985, doi:10.1016/S0967-0645(02)00022-X, 2002.

Matthews, H. D., Gillett, N. P., Stott, P. a and Zickfeld, K.: The proportionality of global warming to cumulative carbon emissions., Nature, 459(7248), 829–32, doi:10.1038/nature08047, 2009.

Mella-Flores, D., Mazard, S., Humily, F., Partensky, F., Mahé, F., Bariat, L., Courties, C., Marie, D., Ras, J., Mauriac, R., Jeanthon, C., Mahdi Bendif, E., Ostrowski, M., Scanlan, D. J. and Garczarek, L.: Is the distribution of Prochlorococcus and Synechococcus ecotypes in the Mediterranean Sea affected by global warming?, Biogeosciences, 8(9), 2785–2804, doi:10.5194/bg-8-2785-2011, 2011.

Middelburg, J. J.: Marine Carbon Biogeochemistry A Primer for Earth System Scientists, Springer B., edited by Springer Briefs in Earth System Sciences, Springer Briefs in Earth System Sciences,., 2019.

Millero, F. J.: Thermodynamics of the carbon dioxide system in the oceans, Geochim. Cosmochim. Acta, 59(4), 661–677, doi:10.1016/0016-7037(94)00354-O, 1995.

Millet, B., Pinazo, C., Daniela, B., Remi, P., Pierre, G. and Ivane, P.: Unexpected spatial impact of treatment plant discharges induced by episodic hydrodynamic events: Modelling Lagrangian transport of fine particles by Northern Current intrusions in the bays of Marseille (France), edited by P. L. Science, PLoS One, 13(4), e0195257 (25p.), doi:10.1371/journal.pone.0195257, 2018.

Millot, C.: The Gulf of Lions hydrodynamics, Cont. Shelf Res., 10(9), 885–894, doi:10.1016/0278-4343(90)90065-T, 1990.

Monterey, G. and Levitus, S.: Seasonal Variability of Mixed Layer Depth for the World Ocean, NOAA Atlas NESDIS 14, Washington, D. C., 1997.

Moran, M. A.: The global ocean microbiome, Sci. Am. Assoc. Adv. Sci., 350(6266), doi:10.1126/science.aac8455, 2015.

Morris, A. W. and Riley, J. P.: The bromide/chlorinity and sulphate/chlorinity ratio in sea water, Deep Sea Res. Oceanogr. Abstr., 13(4), 699–705, doi:10.1016/0011-7471(66)90601-2, 1966.

Mucci, A.: The solubility of calcite and aragonite in seawater at various salinities, temperatures, and one atmosphere total pressure, Am. J. Sci., 283(7), 780–799, doi:10.2475/ajs.283.7.780, 1983.

Orr, J. C., Fabry, V. J., Aumont, O., Bopp, L., Doney, S. C., Feely, R. A., Gnanadesikan, A., Gruber, N., Ishida, A., Joos, F., Key, R. M., Lindsay, K., Maier-Reimer, E., Matear, R., Monfray, P., Mouchet, A., Najjar, R. G., Plattner, G.-K., Rodgers, K. B., Sabine, C. L., Sarmiento, J. L., Schlitzer, R., Slater, R. D., Totterdell, I. J., Weirig, M.-F., Yamanaka, Y. and Yool, A.: Anthropogenic ocean acidification over the twenty-first century and its impact on calcifying organisms, Nature, 437(7059), 681–6, doi:10.1038/nature04095, 2005.

Pairaud, I., Gatti, J., Bensoussan, N., Verney, R. and Garreau, P.: Hydrology and circulation in a coastal area off Marseille: Validation of a nested 3D model with observations, J. Mar. Syst., 88(1), 20–33, doi:10.1016/j.jmarsys.2011.02.010, 2011.

Para, J., Coble, P. G., Charrière, B., Tedetti, M., Fontana, C. and Sempéré, R.: Fluorescence and absorption properties of chromophoric dissolved organic matter (CDOM) in coastal surface waters of the northwestern Mediterranean Sea, influence of the Rhône River, Biogeosciences, 7(12), 4083–4103, doi:10.5194/bg-7-4083-2010, 2010.

Petrenko, A.: Variability of circulation features in the Gulf of Lion NW Mediterranean Sea . Importance of inertial currents Variabilité de la circulation dans le golfe du Lion (Méditerranée nord-occidentale). Importance des courants d ' inertie., Oceanol. Acta, 26, 323–338, doi:10.1016/S0399-1784(03)00038-0, 2003.

Pont, D., Simonnet, J.-P. and Walter, A. V: Medium-term Changes in Suspended Sediment Delivery to the Ocean: Consequences of Catchment Heterogeneity and River Management (Rhône River, France), Estuar. Coast. Shelf Sci., 54(1), 1–18, doi:10.1006/ecss.2001.0829, 2002.

Le Quéré, C., Andrew, R. M., Friedlingstein, P., Sitch, S., Hauck, J., Pongratz, J., Pickers, P. A., Korsbakken, J. I., Peters, G. P., Canadell, J. G., Arneth, A., Arora, V. K., Barbero, L., Bastos, A., Bopp, L., Chevallier, F., Chini, L. P., Ciais, P., Doney, S. C., Gkritzalis, T., Goll, D. S., Harris, I., Haverd, V., Hoffman, F. M., Hoppema, M., Houghton, R. A., Hurtt, G., Ilyina, T., Jain, A. K., Johannessen, T., Jones, C. D., Kato, E., Keeling, R. F., Goldewijk, K. K.,

https://doi.org/10.5194/gmd-2020-41
Preprint. Discussion started: 18 May 2020

620 Landschützer, P., Lefèvre, N., Lienert, S., Liu, Z., Lombardozzi, D., Metzl, N., Munro, D. R., Nabel, J. E. M. S.,
621 Nakaoka, S.-I., Neill, C., Olsen, A., Ono, T., Patra, P., Peregon, A., Peters, W., Peylin, P., Pfeil, B., Pierrot, D.,
622 Poulter, B., Rehder, G., Resplandy, L., Robertson, E., Rocher, M., Rödenbeck, C., Schuster, U., Schwinger, J.,
623 Séférian, R., Skjelvan, I., Steinhoff, T., Sutton, A., Tans, P. P., Tian, H., Tilbrook, B., Tubiello, F. N., van der Laan-
624 Luijkx, I. T., van der Werf, G. R., Viovy, N., Walker, A. P., Wiltshire, A. J., Wright, R., Zaehle, S. and Zheng, B.:
625 Global Carbon Budget 2018, Earth Syst. Sci. Data, 10(4), 2141–2194, doi:10.5194/essd-10-2141-2018, 2018.
626 Raven, J. A. and Falkowski, P. G.: Oceanic sinks for atmospheric CO_2, Plant. Cell Environ., 22(6), 741–755,
627 doi:10.1046/j.1365-3040.1999.00419.x, 1999.
628 Riley, J. P.: The occurrence of anomalously high fluoride concentrations in the North Atlantic, Deep Sea Res.
629 Oceanogr. Abstr., 12(2), 219–220, doi:10.1016/0011-7471(65)90027-6, 1965.
630 Riley, J. P. and Tongudai, M.: The major cation/chlorinity ratios in sea water, Chem. Geol., 2, 263–269,
631 doi:10.1016/0009-2541(67)90026-5, 1967.
632 Roobaert, A., Laruelle, G. G., Landschützer, P., Gruber, N., Chou, L. and Regnier, P.: The Spatiotemporal Dynamics
633 of the Sources and Sinks of CO2 in the Global Coastal Ocean, Global Biogeochem. Cycles, 33,
634 doi:10.1029/2019GB006239, 2019.
635 Ross, O. N., Fraysse, M., Pinazo, C. and Pairaud, I.: Impact of an intrusion by the Northern Current on the
636 biogeochemistry in the eastern Gulf of Lion, NW Mediterranean, Estuar. Coast. Shelf Sci., 170, 1–9,
637 doi:10.1016/j.ecss.2015.12.022, 2016.
638 Rykiel, E. J.: Testing ecological models: The meaning of validation, Ecol. Modell., 90(3), 229–244,
639 doi:10.1016/0304-3800(95)00152-2, 1996.
640 Sarthou, G., Timmermans, K. R., Blain, S. and Tréguer, P.: Growth physiology and fate of diatoms in the ocean: a
641 review, J. Sea Res., 53(1), 25–42, doi:10.1016/j.seares.2004.01.007, 2005.
642 Schneider, A., Wallace, D. W. R. and Körtzinger, A.: Alkalinity of the Mediterranean Sea, Geophys. Res. Lett.,
643 34(15), doi:10.1029/2006GL028842, 2007.
644 Small, C. and Nicholls, R. J.: A Global Analysis of Human Settlement in Coastal Zones, J. Coast. Res., 19(3), 584–
645 599 [online] Available from: http://www.jstor.org/stable/4299200, 2003.
646 Smith, C. L. and Tett, P.: A depth-resolving numerical model of physically forced microbiology at the European
647 shelf edge, J. Mar. Syst., 26(1), 1–36, doi:10.1016/S0924-7963(00)00010-5, 2000.
648 Soetaert, K., Hofmann, A. F., Middelburg, J. J., Meysman, F. J. R. and Greenwood, J.: The effect of biogeochemical
649 processes on pH, Mar. Chem., 105(1–2), 30–51, doi:10.1016/j.marchem.2006.12.012, 2007.
650 Tett, P.: A three-layer vertical and microbiological processes model for shelf seas., 1990.
651 Tett, P., Droop, M. R. and Heaney, S. I.: The Redfield Ratio and Phytoplankton Growth Rate, J. Mar. Biol. Assoc.
652 United Kingdom, 65(2), 487–504, doi:10.1017/S0025315400050566, 1985.
653 Thingstad, T. F.: Utilization of N, P, and organic C by heterotrophic bacteria . I. Outline of a chemostat theory with a
654 consistent concept of "maintenance" metabolism, Mar. Ecol. Prog. Ser., 35, 99–109, doi:10.3354/meps035099, 1987.
655 Uppström, L. R.: The boron/chlorinity ratio of deep-sea water from the Pacific Ocean, Deep Sea Res. Oceanogr.
656 Abstr., 21(2), 161–162, doi:10.1016/0011-7471(74)90074-6, 1974.
657 Upstill-Goddard, R. C.: Air-sea gas exchange in the coastal zone, Estuar. Coast. Shelf Sci., 70(3), 388–404,
658 doi:10.1016/j.ecss.2006.05.043, 2006.
659 Wanninkhof, R. H.: Relationship Between Wind Speed and Gas Exchange, J. Geophys. Res., 97(C5), 7373–7382,
660 1992.
661 Weiss, R. F.: Carbon dioxide in water and seawater: the solubility of a non-ideal gas, Mar. Chem., 2(3), 203–215,
662 doi:10.1016/0304-4203(74)90015-2, 1974.
663 Willmott, C. J.: Some comments on the evaluation of model performance, Bull. Am. Meteorol. Soc., 63(11), 1982.
664 Wimart-Rousseau, C., Lajaunie-Salla, K., Marrec, P., Wagener, T., Raimbault, P., Lagadec, V., Lafont, M., Garcia,
665 N., Diaz, F., Pinazo, C., Yohia, C., Garcia, F., Xueref-Remy, I., Blanc, P. E., Armengaud, A. and Lefèvre, D.:
666 Temporal variability of the carbonate system and air-sea CO_2 exchanges in a Mediterranean human-impacted coastal
667 site, Estuar. Coast. Shelf Sci., 236(February), doi:10.1016/j.ecss.2020.106641, 2020.
668 Xueref-Remy, I., Milne, M., Zoghbi, N., Yohia, C., Armengaud, A., Blanc, P.-E., Delmotte, M., Piazzola, J., Nathan,
669 B., Ramonet, M. and Lac, C.: Assessing atmospheric CO_2 variability in the Aix-Marseille metropolis area (France)
670 and its coastal Mediterranean Sea at different time scales within the AMC project, Prague, Aus, [online] Available
671 from: https://conference.icos-ri.eu/wp-ontent/uploads/2018/09/ICOS2018SC_Book_of_Abstracts.pdf, 2018a.
672 Xueref-Remy, I., Dieudonné, E., Vuillemin, C., Lopez, M., Lac, C., Schmidt, M., Delmotte, M., Chevallier, F.,
673 Ravetta, F., Perrussel, O., Ciais, P., Bréon, F., Broquet, G., Ramonet, M. and Ampe, C.: Diurnal , synoptic and
674 seasonal variability of atmospheric CO_2 in the Paris megacity area, Atmos. Chem. Phys., 18, 3335–3362,
675 doi:10.5194/acp-18-3335-2018, 2018b.
676 Yohia, C.: Genèse du mistral par interaction barocline et advection du tourbillon potentiel, Climatologie, 13, 24–37
677 [online] Available from: https://doi.org/10.4267/climatologie.1182, 2017.
678 Zappa, C. J., Raymond, P. A., Terray, E. A. and McGillis, W. R.: Variation in Surface Turbulence and the Gas

https://doi.org/10.5194/gmd-2020-41
Preprint. Discussion started: 18 May 2020

679 Transfer Velocity over a Tidal Cycle in a Macro-tidal Estuary, Estuaries, 26(6), 1401–1415, 2003.
680
681

https://doi.org/10.5194/gmd-2020-41
Preprint. Discussion started: 18 May 2020

Geoscientific Model Development Discussions

682 **Tables**

	Temperature	Wind	River input	Atmospheric CO_2
S0 – Reference	In situ data of 2017	WRF model 2017	No	CAV station 2017
S1 - T increases	In situ data of 2017 +1.5°C	WRF model 2017	No	CAV station 2017
S2 - Wind constant	In situ data of 2017	7 m s^{-1}	No	CAV station 2017
S3 - Wind events	In situ data of 2017	3 days of 20 m s^{-1}	No	CAV station 2017
S4 - NO_3	In situ data of 2017	WRF model 2017	NO_3 inputs	CAV station 2017
S5 – TA	In situ data of 2017	WRF model 2017	TA inputs	CAV station 2017
S6 - Non-urban	In situ data of 2017	WRF model 2017	No	OHP station 2017

683 **Table 1: Forcing of the different scenarios (S) simulated with the model. See section 2.4 for details of scenarios.**

684

	Chl	sea pCO_2	pH	DIC	TA
Obs min-max	[0.10– 1.71]	[358 – 471]	[8.014 – 8.114]	[2260 – 2348]	[2561 – 2624]
Mod min-max	[0.03 – 0.73]	[331 – 522]	[7.979 – 8.171]	[2220 – 2323]	[2560– 2572]
Bias	-0.22	22.47	-0.016	-8.48	-24.91
WSS	0.36	0.69*	0.75*	0.71*	0.43
N	22	20	21	20	20

685 **Table 2: Statistical evaluation of observations vs. model for 2017 year: observed and simulated minimum and maximum**
686 **values, WSS = Wilmott Skill Score, N = number of measurements. Units of bias are those of modeled variables:**
687 **chlorophyll (Chl, mg m^{-3}), seawater pressure of CO_2 (seawater pCO_2, µatm), *p*H, dissolved inorganic carbon (DIC, µmol**
688 **kg^{-1}) and total alkalinity (TA, µmol kg^{-1}) . *significant value of WSS (> 0.70).**

689

		Aeration	GPP	R_A	R_H	R	NEP
	Year	0.017	-0.413	0.065	0.348	0.413	0
Mean flux	**MWC**	-0.245	-0.314	0.052	0.176	0.228	0.086
	SWC	0.405	-0.521	0.079	0.555	0.634	-0.113
Contribution	**Year**	78%	11%	2%	9%	11%	/

690 **Table 3: Mean flux values (mmol m^{-3} d^{-1}) and the contribution of each process to the DIC variations for the reference**
691 **simulation over the year and SWC/MWC periods. GPP: Gross primary production, R_A: Autotroph respiration, R_H:**
692 **heterotroph respiration, NEP: Net Ecosystem Production**

https://doi.org/10.5194/gmd-2020-41
Preprint. Discussion started: 18 May 2020

Geoscientific Model Development
Discussions
Open Access
EGU

693 **Figures**

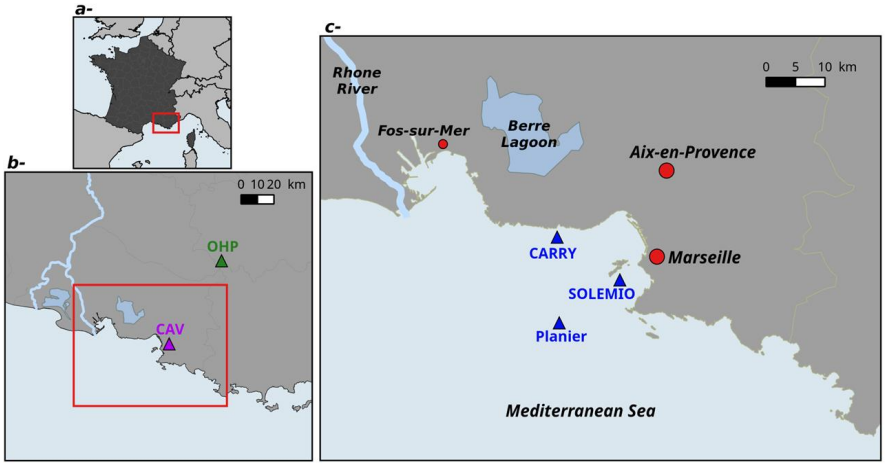

694
695 **Figure 1: Map of study area: The Region Sud (A), Aix-Marseille Metropolis (B), the Bay of Marseille (C). CAV= Cinq**
696 **AVenues Station (urban site), OHP: Observatoire de Haute Provence station (non-urban site), Carry, Solemio, Planier:**
697 **Study sites at sea in the Bay of Marseille.**

698

https://doi.org/10.5194/gmd-2020-41
Preprint. Discussion started: 18 May 2020

Geoscientific Model Development
Discussions
Open Access
EGU

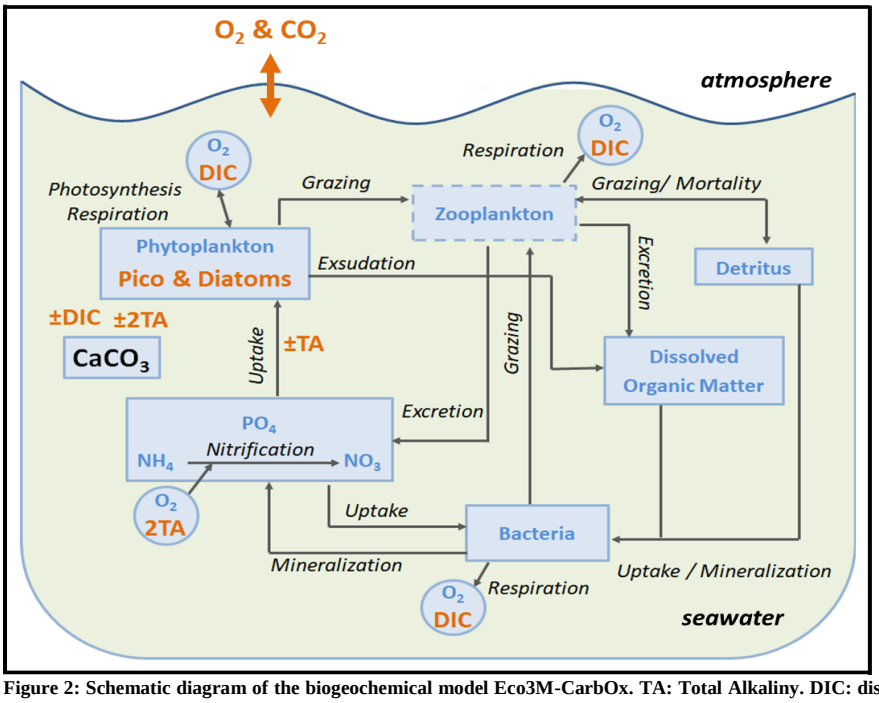

699
700 **Figure 2: Schematic diagram of the biogeochemical model Eco3M-CarbOx. TA: Total Alkaliny. DIC: dissolved inorganic**
701 **carbon.**

702

https://doi.org/10.5194/gmd-2020-41
Preprint. Discussion started: 18 May 2020

Geoscientific Model Development Discussions
Open Access
EGU

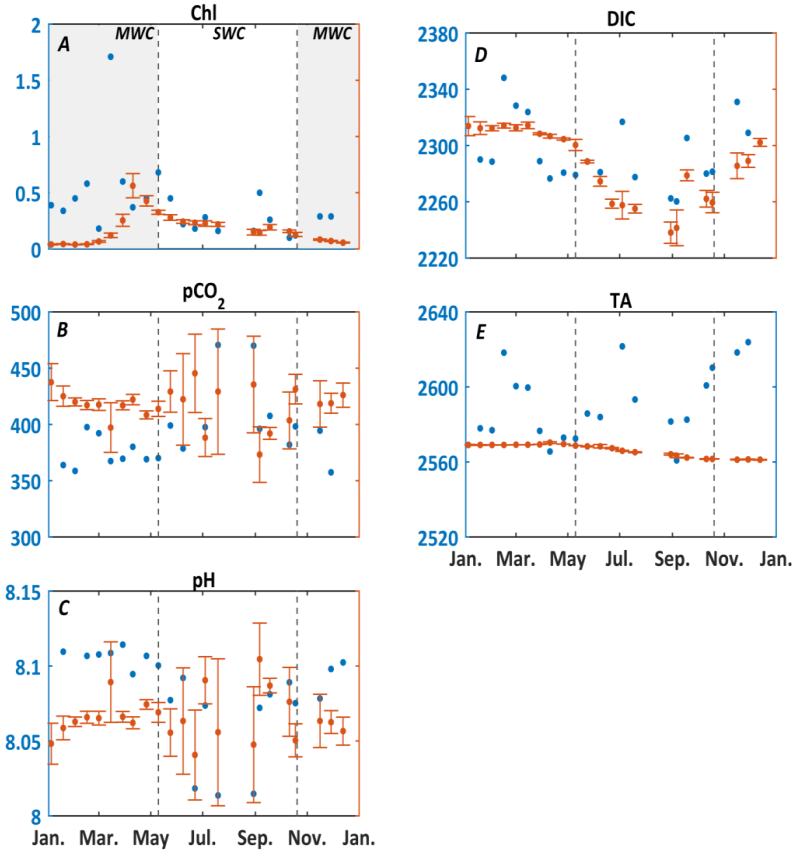

Figure 3: Comparison of model results (red) and *in situ* data (blue) at the SOLEMIO station. (A) Chlorophyll-a concentrations (mg m^{-3}), (B) pCO_2 (µatm), (C) *p*H, (D) DIC (µmol kg^{-1}), (E) TA (µmol kg^{-1}). The value of each state variable represents the mean around ±5 days of the sampling date, and the error bars are the standard deviation of values over this time period. The shaded area and dotted black line delimit the SWC and MWC periods.

https://doi.org/10.5194/gmd-2020-41
Preprint. Discussion started: 18 May 2020

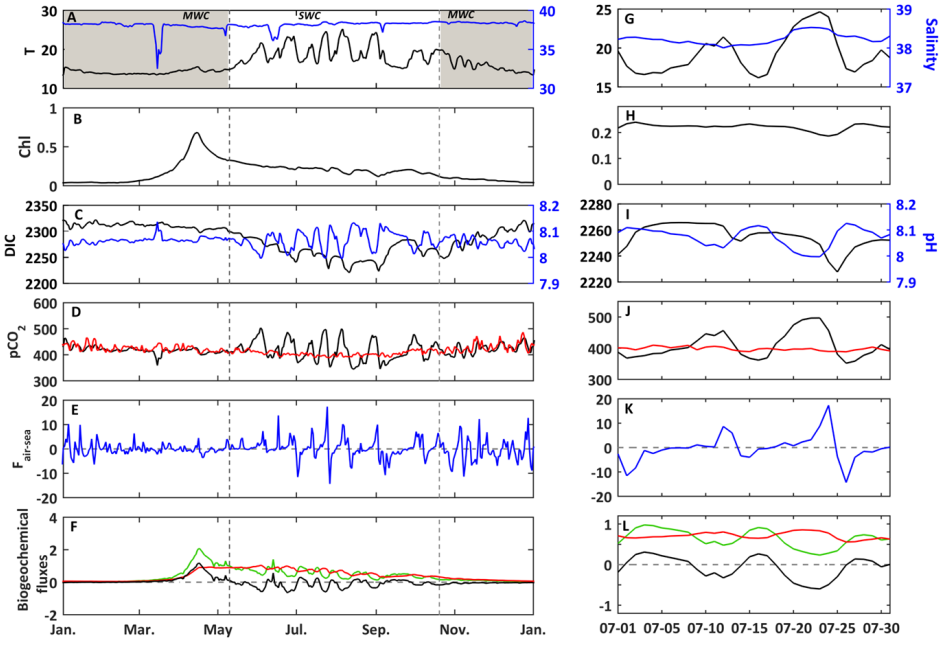

Figure 4: **In the left panels: year 2017 and right panels: temporal focus between July 1st and August 1st, 2017. *In situ* daily average of (A, G) temperature (°C, black line) and salinity (blue line) at the SOLEMIO station. Modeled daily average (B, H) chlorophyll concentrations (mg m^{-3}, black line) (C, I) DIC (µmol kg^{-1}, black line) and *p*H (blue line), (D, J) seawater pCO_2 (µatm, black line) and atmosphere pCO_2 from OHP (µatm, red line), (E, K) air-sea CO_2 fluxes mmol m^{-3} d^{-1}), (F, L) Gross Primary Production (mmol m^{-3} d^{-1}, green line), total respiration (mmol m^{-3} d^{-1}, red line) and Net Ecosystem Production (mmol m^{-3} d^{-1}, black line). The shaded areas and dotted black lines delimit the SWC and MWC periods.**

https://doi.org/10.5194/gmd-2020-41
Preprint. Discussion started: 18 May 2020

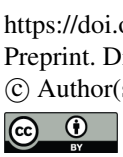

Geoscientific Model Development
Discussions
Open Access
EGU

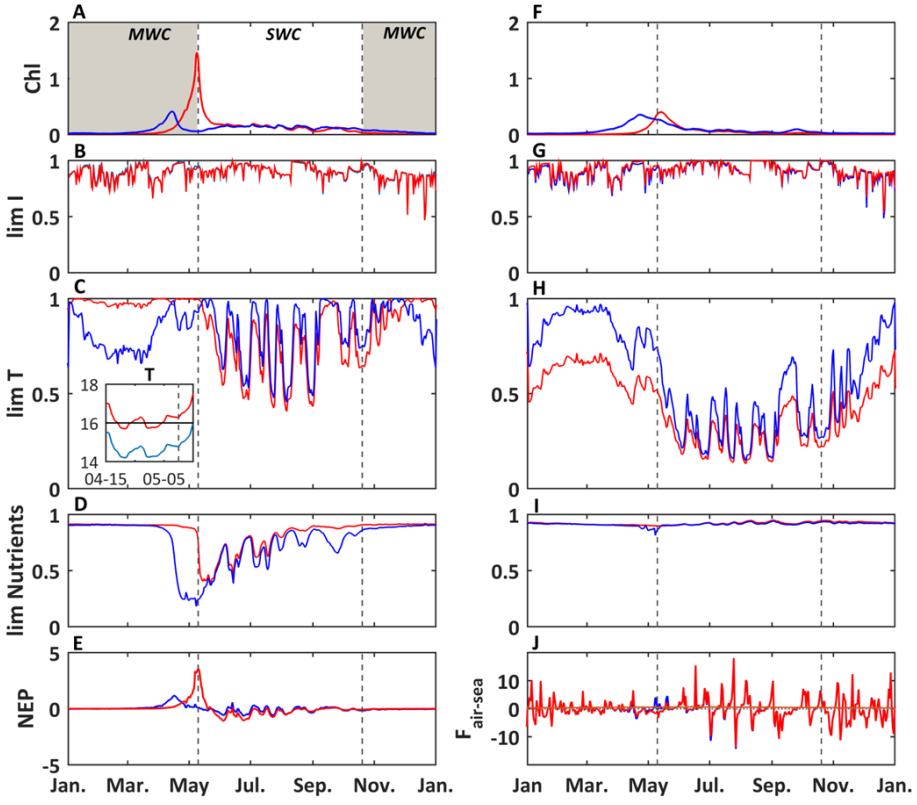

Figure 5: Modeled daily average chlorophyll concentrations (mg m^{-3}) (A), light limitation (B), temperature limitation, and a zoom from April 15th to May 5th of temperature (C) and nutrient limitation (D) for picophytoplankton and the same set for diatoms (F, G, H and I). Modeled daily average NEP (mmol $m^{-3} \cdot d^{-1}$, E) and air-sea CO_2 flux (mmol $m^{-3} \cdot d^{-1}$, J). Reference simulation (S0, blue line) and temperature-shifted simulation by 1.5°C (S2, red line). The shaded area and dotted black lines delimit the SWC and MWC periods.

https://doi.org/10.5194/gmd-2020-41
Preprint. Discussion started: 18 May 2020

Geoscientific Model Development Discussions
Open Access
EGU

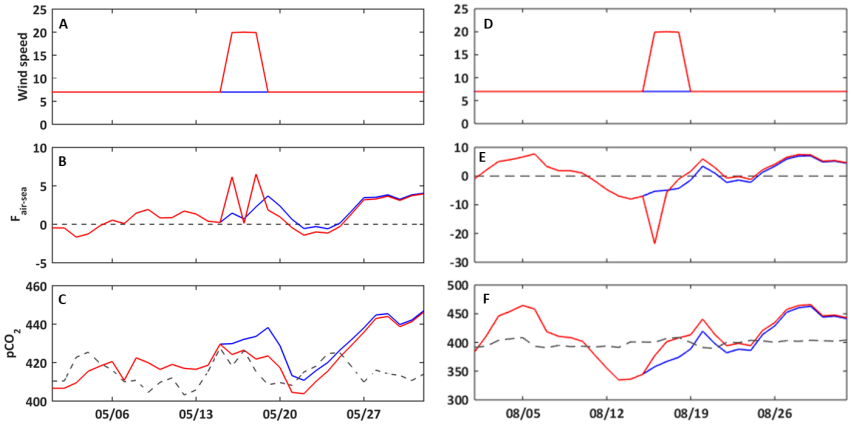

Figure 6: Temporal evolution for May (left panels) and August (right panels) 2017 of the wind speed (m s^{-1}, A, D); air-sea CO_2 fluxes (mmol $m^{-3}.d^{-1}$, B, E); seawater partial pressure of CO_2 (µatm, C, F). Constant wind scenario (S2, blue line) and wind event scenario (S3, red line). On panels C and F, the dashed line represents the atmosphere partial pressure of CO_2 (µatm) at the CAV station.

https://doi.org/10.5194/gmd-2020-41
Preprint. Discussion started: 18 May 2020

Geoscientific Model Development
Discussions
Open Access
EGU

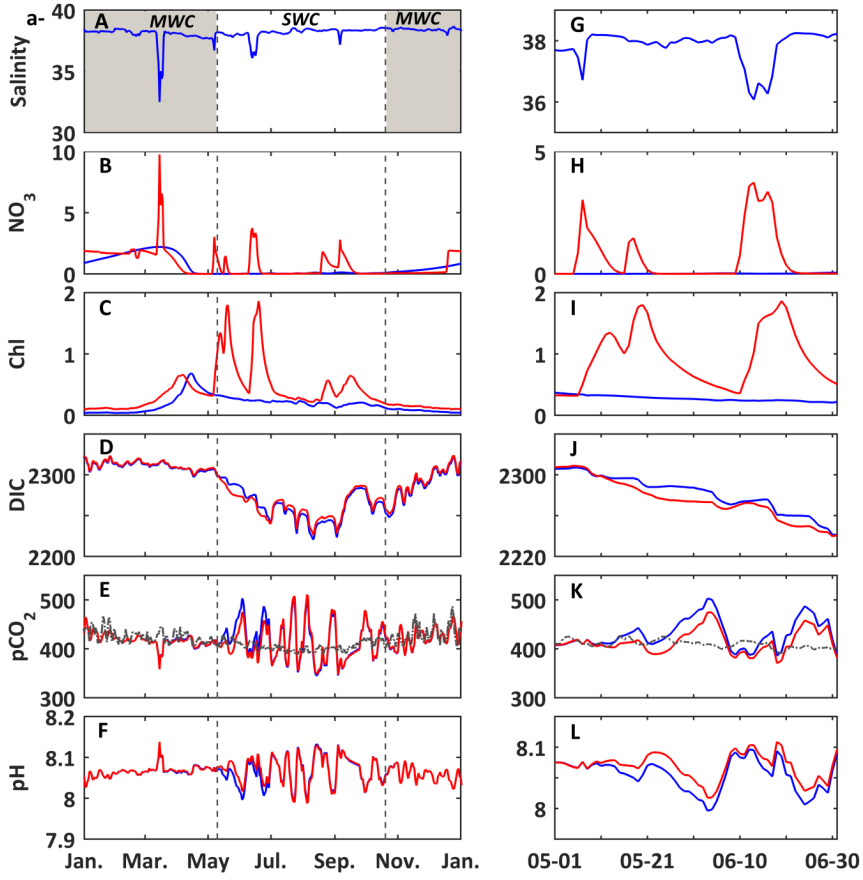

Figure 7: In the left panels: year 2017 and right panels: temporal focus between May 1st and July 1st, 2017. (A, G) *In situ* daily average of salinity. Modeled daily average (B, H) nitrate concentrations (mmol m^{-3}); (C, I) chlorophyll concentrations (mg m^{-3}); (D, J) DIC (µmol kg^{-1}); (E, K) seawater pCO_2 (µatm), and (F, L) *p*H. Reference simulation (S0, blue line) and nitrate supply simulation (S4, red line). On panels E and K, the dashed line represents the atmosphere partial pressure of CO_2 (µatm) at the CAV station. The shaded area and dotted black lines delimit the SWC and MWC periods.

https://doi.org/10.5194/gmd-2020-41
Preprint. Discussion started: 18 May 2020

Geoscientific Model Development
Discussions
Open Access
EGU

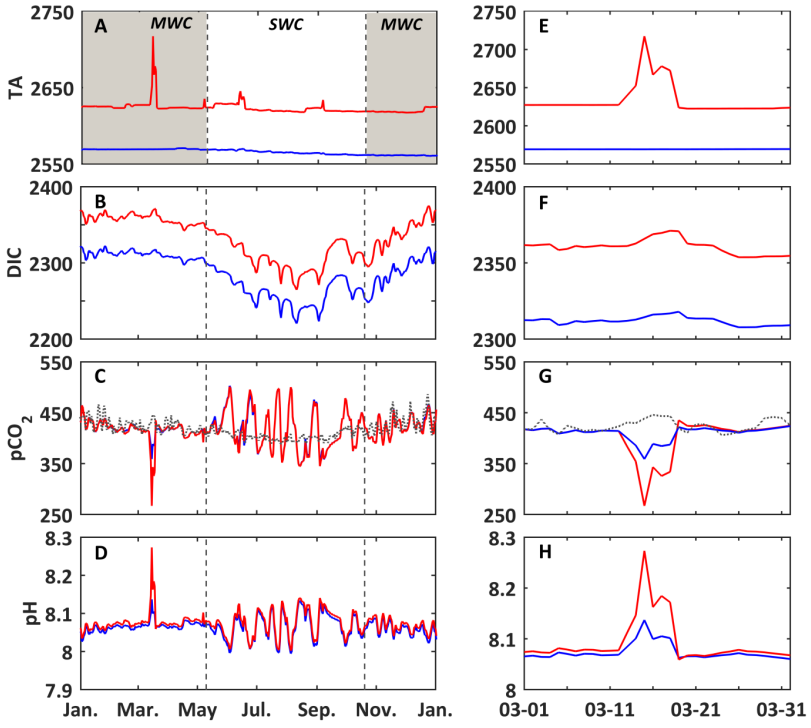

738
739 **Figure 8: In the left for the whole year 2017 and in the right between March 1st and April 1st, 2017. Modelled daily**
740 **average (A, E) TA (µmol kg^{-1}); (B, F) DIC (µmol kg^{-1}); (C, G) seawater pCO_2 (µatm), and (D, H) pH. Reference simulation**
741 **(S0, blue line) and alkalinity supply simulation (S5, red line). On the panels C and G, the dashed line represents the**
742 **atmosphere partial pressure of CO_2 (µatm) at the CAV station. The shaded area and dotted black lines delimit the SWC**
743 **and MWC periods.**

744

https://doi.org/10.5194/gmd-2020-41
Preprint. Discussion started: 18 May 2020

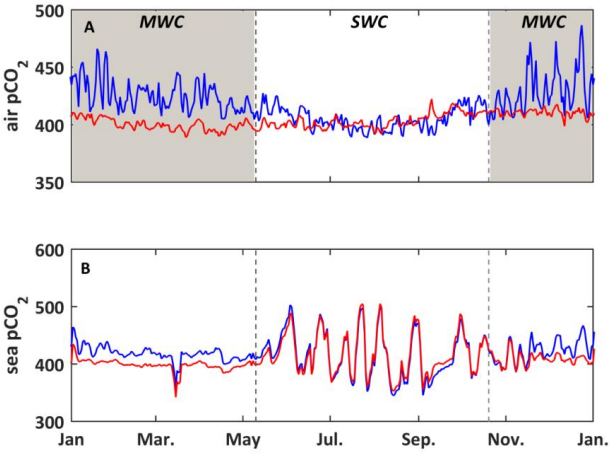

745
746 **Figure 9: (A) Temporal evolution for the year 2017 of the observed partial pressure of CO_2 in the atmosphere in µatm at**
747 **the CAV station, called the "urban scenario" (S0, blue line), and at the OHP station, called the "non-urban scenario", and**
748 **seawater (S6, red line). (B) Temporal evolution for the year 2017 of the modeled seawater partial pressure of CO_2 (µatm)**
749 **with forcings from the urban (S0, blue line) and non-urban (S6, red line) scenarios. The shaded area and dotted black lines**
750 **delimit the SWC and MWC periods.**

https://doi.org/10.5194/gmd-2020-41
Preprint. Discussion started: 18 May 2020

Geoscientific Model Development Discussions

Appendix

Table A1: Initial conditions of the state variables of Eco3M-CarbOx model (*diagnostic variables)

Variables	Name	Unit	values
Picophytoplankton	$PicoC$	mmolC m^{-3}	0.0480
	$PicoN$	mmolN m^{-3}	0.0092
	$PicoP$	mmolP m^{-3}	0.0003
Diatom	$DiaC$	mmolC m^{-3}	0.0571
	$DiaN$	mmolN m^{-3}	0.0089
	$DiaP$	mmolP m^{-3}	0.0007
Bacteria	$BacC$	mmolC m^{-3}	0.1083
	$BacN$	mmolN m^{-3}	0.0379
	$BacP$	mmolP m^{-3}	0.0039
Detritus or POM Particulate organic matter	POC	mmolC m^{-3}	0.1252
	PON	mmolN m^{-3}	0.0307
	POP	mmolP m^{-3}	0.0021
DOM Dissolved organic matter	DOC	mmolC m^{-3}	1.0990
	DON	mmolN m^{-3}	8.7980
	DOP	mmolP m^{-3}	0.0018
DIM Dissolved inorganic matter	NH_4	mmolN m^{-3}	0.3375
	NO_3	mmolN m^{-3}	0.6723
	PO_4	mmolP m^{-3}	0.7150
	DO	mmolO m^{-3}	257.00
	DIC	µmolC kg^{-1}	2358.4
Total alkalinity	TA	µmolC kg^{-1}	2660.5
Sea water partial pressure of CO_2	pCO_2	µatm	371.28
***p*H**	*p*H	/	8.1099
calcium carbonate	$CaCO_3$	mmol m^{-3}	1.0000
Picophytoplankton chlorophyll*	*PicoChl*	mgChl m^{-3}	0.0193
Diatom chlorophyll*	*DiaChl*	mgChl m^{-3}	0.0229
Number of bacteria*	NBA	10^{12} cell m^{-3}	0.2000

https://doi.org/10.5194/gmd-2020-41
Preprint. Discussion started: 18 May 2020

Geoscientific Model Development Discussions

755 **Table A2: Balance equations of Eco3M-CarbOx model**

Variables	Balance equation
Picophytoplankton	$\frac{\partial PicoC}{\partial t} = R_{PP}^{Pico} - R_{resp}^{Pico} - R_{exsu}^{PicoC} - R_{Gr}$ $\frac{\partial PicoN}{\partial t} = R_{uptNH_4} + R_{uptNO_3} - R_{exsu}^{PicoN} - R_{Gr}$ $\frac{\partial PicoP}{\partial t} = R_{uptPO_4} - R_{exsu}^{PicoP} - R_{Gr}$ $PicoChl = Q_C^N \cdot \left(Q_{N,min}^{Chla} + f_Q^N \cdot \left(Q_{N,max}^{Chla} - Q_{N,min}^{Chla}\right)\right) \cdot PicoC$
Diatom	$\frac{\partial DiaC}{\partial t} = R_{PP}^{Dia} - R_{resp}^{Dia} - R_{exsu}^{DiaC} - R_{Gr}$ $\frac{\partial DiaN}{\partial t} = R_{uptNH_4} + R_{uptNO_3} - R_{exsu}^{DiaN} - R_{Gr}$ $\frac{\partial DiaP}{\partial t} = R_{uptPO_4} - R_{exsu}^{DiaP} - R_{Gr}$ $DiaChl = Q_C^N \cdot \left(Q_{N,min}^{Chla} + f_Q^N \cdot \left(Q_{N,max}^{Chla} - Q_{N,min}^{Chla}\right)\right) \cdot DiaC$
Bacteria	$\frac{\partial BacC}{\partial t} = R_{uptBac}^{POC} + R_{uptBac}^{DOC} - R_{BR} - R_{Gr}^{BacC}$ $\frac{\partial BacN}{\partial t} = R_{uptBac}^{PON} + R_{uptBac}^{DON} + R_{uptBac}^{NH4} - R_{miner}^{NH4} - R_{Gr}^{BacN}$ $\frac{\partial BacP}{\partial t} = R_{uptBac}^{POP} + R_{uptBac}^{DOP} + R_{uptBac}^{PO4} - R_{miner}^{PO4} - R_{Gr}^{BacP}$
Detritus	$\frac{\partial POC}{\partial t} = R_{pf} + R_m - R_{Gr} - R_{uptBac}^{POC}$ $\frac{\partial PON}{\partial t} = R_{pf} + R_m - R_{Gr} - R_{uptBac}^{PON}$ $\frac{\partial POP}{\partial t} = R_{pf} + R_m - R_{Gr} - R_{uptBac}^{POP}$
MOD	$\frac{\partial DOC}{\partial t} = R_{exsu}^{PicoC} + R_{exsu}^{DiaC} + R_{excr}^{DOC} - R_{uptBac}^{DOC}$ $\frac{\partial DON}{\partial t} = R_{exsu}^{PicoN} + R_{exsu}^{DiaN} + R_{excr}^{DON} - R_{uptBac}^{DON}$ $\frac{\partial DOP}{\partial t} = R_{exsu}^{PicoP} + R_{exsu}^{DiaP} + R_{excr}^{DOP} - R_{uptBac}^{DOP}$
NH_4	$\frac{\partial NH_4}{\partial t} = R_{excr}^{NH_4} + R_{miner}^{NH_4} - R_{nit} - \sum R_{uptPhyN}^{NH_4} - R_{uptBac}^{NH_4}$
NO_3	$\frac{\partial NO_3}{\partial t} = R_{nit} - \sum R_{uptPhyN}^{NO_3} \cdot \left(1 - \frac{I_{in}.NH_4}{NH_4 + K_{in}}\right)$
PO_4	$\frac{\partial PO_4}{\partial t} = R_{excr}^{PO_4} + R_{miner}^{PO_4} - \sum R_{uptPhyP}^{PO_4} - R_{uptBac}^{PO_4}$
DO	$\frac{\partial DO}{\partial t} = R_{aera} + \left(\frac{O}{C}\right)_{PP} \cdot R_{PP}^{Phy} + \left(\frac{O}{N}\right)_{uptNO_3} \cdot R_{uptNO_3}^{PhyN} - \left(\frac{O}{C}\right)_{resp} \cdot R_{resp} - \left(\frac{O}{C}\right)_{respZ} \cdot R_{excr}^{DIC} - \left(\frac{O}{C}\right)_{respBa} \cdot R_{BR} - \left(\frac{O}{N}\right)_{nit} \cdot R_{nit}$

https://doi.org/10.5194/gmd-2020-41
Preprint. Discussion started: 18 May 2020

Geoscientific Model Development Discussions
Open Access
EGU

DIC	$\frac{\partial DIC}{\partial t} = R_{aera} + R_{resp}^{Phy} + R_{BR} + R_{excr}^{DIC} - R_{PP}^{Phy} - R_{precip} + R_{diss}$
TA	$\frac{\partial TA}{\partial t} = 2 \cdot R_{diss} + \left(R_{uptPhyN}^{NO_3} + R_{uptPhyP}^{PO_4} - R_{uptPhyN}^{NH_4}\right) + R_{miner}^{NH_4} - 2 \cdot R_{precip} - 2.R_{nit}$

https://doi.org/10.5194/gmd-2020-41
Preprint. Discussion started: 18 May 2020

Geoscientific Model Development Discussions

Table A3: Biogeochemical processes simulated by Eco3M-CarbOx

Notation	Biogeochemical processes	Unit	Formulation	
$\boldsymbol{R_{PP}^{Phy}}$	Primary production	molC m^{-3} s^{-1}	$R_{PP}^{Phy} = P_m^C \cdot f_T^{PP} \cdot f_I \cdot PhyC$	$P_m^C = P_{max} \cdot f_Q \cdot f_T^{PP}$; $f_Q = min\left[f_Q^N, f_Q^P\right]$; $f_Q^X = \frac{Q_C^X - Q_{C,min}^X}{Q_C^X - Q_{C,min}^X + \beta_X}$ $f_T^{PP} = max\left(\frac{2\cdot(1-b)\cdot\frac{(T-T_{let})}{(T_{opt}-T_{let})}}{\left(\frac{(T-T_{let})}{(T_{opt}-T_{let})}\right)^2 - 2\cdot b\cdot\frac{(T-T_{let})}{(T_{opt}-T_{let})}+1}; 0\right)$ $f_I = \left[1 - exp\left(\frac{-\alpha_{Chla}\cdot E_{PAR}\cdot Q_C^{Chla}}{P_m^C}\right)\right]$
$\boldsymbol{R_{resp}^{Phy}}$	Phytoplankton respiration	molC m^{-3} s^{-1}	$R_{resp}^{Phy} = k_r^{PhyC} \cdot PhyC$	
$\boldsymbol{R_{uptX}^{Phy}}$	Nutrients uptake by phytoplankton	molX m^{-3} s^{-1}	$R_{uptX}^{Phy} = V_{N,max} \cdot \frac{X}{X + K_X}$	$V_{N,max} = Q_{C,max}^X \cdot R_{PP}^{Phy}$
$\boldsymbol{R_{exsu}^{PhyC}}$	Phytoplankton exudation as DIC	molC m^{-3} s^{-1}	$R_{exsu}^{PhyC} = \left(1 - f_Q\right) \cdot R_{PP}^{Phy}$	
$\boldsymbol{R_{exsu}^{PhyX}}$	Phytoplankton exudation as NH_4 or PO_4	molX m^{-3} s^{-1}	$R_{exsu}^{PhyX} = \left(1 - h_Q^X\right) \cdot R_{uptX}^{Phy}$	$h_Q^X = \frac{Q_{C,max}^X - Q_C^X}{Q_{C,max}^X - Q_{C,min}^X}$
$\boldsymbol{R_{BP}}$	Bacterial production	cell m^{-3} s^{-1}	$R_{BP} = \mu_{max}^{Ba} \cdot f_Q^{Ba} \cdot f_T^{Ba} \cdot NBA$	$f_T^{Ba} = Q_{10}^{\frac{(T-T_{rem})}{10}}$; $f_Q^{BA} = min\left[1 - \frac{Q_{C,min}^{BA}}{Q_C^{BA}}, 1 - \frac{Q_{N,min}^{BA}}{Q_N^{BA}}, 1 - \frac{Q_{P,min}^{BA}}{Q_P^{BA}}\right]$
$\boldsymbol{R_{BR}}$	Bacterial respiration	molC m^{-3} s^{-1}	$R_{BR} = \rho_g^{Ba}.Q_C^{Ba}.R_{BP} + \rho_r^{Ba}.\left(Q_C^{Ba} - Q_{C,min}^{Ba}\right).NBA$	
$\boldsymbol{R_{uptBac}^{X}}$	X uptake by bacteria	molX m^{-3} s^{-1}	$R_{uptBac}^{X} = V_{max}^{BA} \cdot \frac{X}{X + K_X^{Ba}} \cdot f_T^{Ba} \cdot NBA$	
$\boldsymbol{R_{Gr}^{Phy}}$	Phytoplankton grazing by zooplankton	molX m^{-3} s^{-1}	$R_{Gr}^{Phy} = g_{Phy} \cdot f_{Gr} \cdot Phy$	$f_{Gr} = \frac{Phy}{Phy + POM}$
$\boldsymbol{R_{Gr}^{POM}}$	Detritus grazing by zooplankton	molX m^{-3} s^{-1}	$R_{Gr}^{POM} = g_{POM} \cdot f_{Gr} \cdot POM$	$g_{POM} = \frac{g_{Pico}\cdot Pico + g_{Dia}\cdot Dia}{Pico + Dia}$; $f_{Gr} = \frac{POM}{Phy + POM}$
$\boldsymbol{R_{Gr}^{Bac}}$	Bacterial grazing by zooplankton	molX m^{-3} s^{-1}	$R_{Gr}^{Ba} = R_{BP} \cdot \frac{Bac}{NBA}$	
$\boldsymbol{R_{excr}^{DIM}}$	Zooplankton excretion as DIC, NH_4 and PO_4	molX m^{-3} s^{-1}	$R_{excr}^{DIM} = \varepsilon_{DIM} \cdot d_X \cdot \left(1 - k_{X,zoo}\right) \cdot \left(R_{Gr}^{Phy} + R_{Gr}^{POM} + R_{Gr}^{Ba}\right)$	

https://doi.org/10.5194/gmd-2020-41
Preprint. Discussion started: 18 May 2020

Geoscientific Model Development Discussions

$\boldsymbol{R_{excr}^{DOM}}$	Zooplankton excretion as DOM	molX m^{-3} s^{-1}	$R_{excr}^{DOM} = (1 - \varepsilon_{DIM}) \cdot d_X \cdot (1 - k_{X,zoo}) \cdot (R_{Gr}^{Phy} + R_{Gr}^{POM} + R_{Gr}^{Ba})$	
$\boldsymbol{R_{pf}}$	Zooplankton egestion	molX m^{-3} s^{-1}	$R_{pf} = (1 - d_X) \cdot (R_{Gr}^{Phy} + R_{Gr}^{POM} + R_{Gr}^{Ba})$	
$\boldsymbol{R_{m}}$	Zooplankton mortality	molX m^{-3} s^{-1}	$R_{m} = d_X \cdot k_{X,zoo} \cdot (R_{Gr}^{Phy} + R_{Gr}^{POM} + R_{Gr}^{Ba})$	
$\boldsymbol{R_{miner}}$	Mineralization of organic matter by bacteria	molX m^{-3} s^{-1}	$R_{miner}^{X} = (1 - h_Q^{Ba}) \cdot (R_{uptBac}^{DOM} + R_{uptBac}^{POM} + R_{uptBac}^{DIM})$	
$\boldsymbol{R_{nit}}$	Nitrification	molX m^{-3} s^{-1}	$R_{nit} = k_{nit} \cdot f_T^{Ba} \cdot \frac{DO}{DO + K_{DO}} \cdot NH_4$	
$\boldsymbol{R_{diss}}$	Carbonate dissolution	molC m^{-3} s^{-1}	$R_{diss} = (1 - \Omega_C) \cdot k_{diss} \cdot [CaCO_3]$	Ω_C =aragonite saturation
$\boldsymbol{R_{precip}}$	Carbonate precipitation	molC m^{-3} s^{-1}	$R_{precip} = k_{precip} \cdot \frac{(\Omega_C - 1)}{K_C + (\Omega_C - 1)} \cdot (R_{PP}^{Phy} - R_{resp}^{Phy})$	
$\boldsymbol{R_{aera}}$	Gas exchange with atmosphere of DO or CO_2	molX m^{-3} s^{-1}	$R_{aera} = \frac{k_{ex}}{H} \cdot ([DO]_{sea} - [DO]_{sat})$ $R_{aera} = \frac{k_{ex}}{H} \cdot \alpha \cdot (pCO_{2,sea} - pCO_{2,atm})$	$k_{ex} = 0.31 \cdot U_{10}^2 \cdot \frac{660}{Sc}^{0.5}$ H (depth), U_{10}(wind velocity) α (solubility), Sc (Schmidt number) and $[DO]_{sat}$ are function of T and S

https://doi.org/10.5194/gmd-2020-41
Preprint. Discussion started: 18 May 2020

Geoscientific Model Development Discussions

760 **Table A4: Value of parameters**

Parameters		Pico	Dia	Unit	Reference
P_m^C	Maximal production	1.815	1.057	d^{-1}	Sarthou et al. (2005)
m_1	Fraction of the solar energy flux photosynthetically available	0.43	0.43	/	Tett (1987)
m_2	Sea surface reflection	0.95	0.95	/	Tett (1987)
m_3	More rapid attenuation of polychromatic light near the sea surface	1.0	1.0	/	Tett (1987)
α_{Chla}	Chlorophyll-specific light absorption coefficient	$8\ 10^{-6}$	$5\ 10^{-6}$	m^2 molC $(gChla\ J)^{-1}$	Leblanc et al. (2018)
T_{opt}	Temperature optimal of growth	16.0	13.0	°C	/
T_{let}	Lethal temperature	11.0	9.0	°C	/
b	Shape factor for temperature curve	0.5	0.8	/	Lacroix and Grégoire (2002)
β_N	Coefficient in the quota function	0.0072	0.002	molN $molC^{-1}$	Leblanc et al. (2018)
β_P	Coefficient in the quota function	0.0002	0.0005	molP $molC^{-1}$	Leblanc et al. (2018)
$Q_{C,min}^N$	Minimum phytoplankton N:C ratio	0.115	0.07	molN $molC^{-1}$	Leblanc et al. (2018)
$Q_{C,max}^N$	Maximum phytoplankton N:C ratio	0.229	0.18	molN $molC^{-1}$	Leblanc et al. (2018)
$Q_{C,min}^P$	Minimum phytoplankton P:C ratio	0.0015	0.006	molP $molC^{-1}$	Auger et al. (2011); Campbell et al. (2013)
$Q_{C,max}^P$	Maximum phytoplankton P:C ratio	0.0068	0.016	molP $molC^{-1}$	Auger et al. (2011); Campbell et al. (2013)
$Q_{N,min}^{Chla}$	Minimum phytoplankton Chl:N ratio	1.0	1.0	gChl $molN^{-1}$	Leblanc et al. (2018)**
$Q_{N,max}^{Chla}$	Maximum phytoplankton Chl:N ratio	2.2	2.7	gChl $molN^{-1}$	Leblanc et al. (2018)
k_r^{PhyC}	Phytoplankton respiration rate	0.099	0.099	d^{-1}	Faure et al. (2010)
K_{NO_3}	Half saturation constant for NO_3	0.73	1.0	mmolN m^{-3}	Leblanc et al. (2018)
K_{NH_4}	Half saturation constant for NH_4	0.07	0.015	mmolN m^{-3}	Calibrated
K_{PO_4}	Half saturation constant for PO_4	0.008	0.01	mmolP m^{-3}	Leblanc et al. (2018)**
I_{in}	Factor of inhibition	0.82	0.82	/	Harrison et al. (1996)
K_{in}	Amount of NH_4 from which assimilation by NO_3 is reduced.	0.578	0.578	mmolN m^{-3}	Harrison et al. (1996)
g	Grazing rate	1.452	0.846	d^{-1}	Gutiérrez-Rodríguez et al. (2011)

** calibrated

https://doi.org/10.5194/gmd-2020-41
Preprint. Discussion started: 18 May 2020

Geoscientific Model Development Discussions

Table A5: Value of parameters (continue)

Parameters		Value	Unit	Reference
NBA	Number of bacteria	0.20	10^{12} cell m^{-3}	Moran (2015)
μ_{max}^{Ba}	Bacterial production rate	8.36	d^{-1}	Fraysse et al. (2013)
$Q_{C,min}^{BA}$	Minimum bacteria C:cell ratio	0.49	mmolC (10^{12} cell)$^{-1}$	Fukuda et al. (1998)
$Q_{N,min}^{BA}$	Minimum bacteria N:cell ratio	0.09	mmolN (10^{12} cell)$^{-1}$	Fukuda et al. (1998)
$Q_{N,max}^{BA}$	Maximum bacteria N:cell ratio	0.23	mmolN (10^{12} cell)$^{-1}$	Fukuda et al. (1998)
$Q_{P,min}^{BA}$	Minimum bacteria P:cell ratio	0.005	mmolP (10^{12} cell)$^{-1}$	Fraysse et al. (2013)
$Q_{P,max}^{BA}$	Maximum bacteria P:cell ratio	0.02	mmolP (10^{12} cell)$^{-1}$	Fraysse et al. (2013)
ρ_g^{Ba}	Factor of carbon respired by bacteria	0.60	/	Thingstad (1987)
ρ_r^{Ba}	Respiration rate of bacteria	0.01	d^{-1}	Thingstad (1987)
$V_{DOC,max}^{BA}$	Maximum POC uptake by bacteria	0.029	mmolC (10^{12}cell)$^{-1}$ d^{-1}	Campbell et al. (2013)
$V_{DOC,max}^{BA}$	Maximum DOC uptake by bacteria	16.33	mmolC (10^{12} cell)$^{-1}$ d^{-1}	Campbell et al. (2013)
$V_{PON,max}^{BA}$	Maximum PON uptake by bacteria	0.05	mmolN (10^{12} cell)$^{-1}$ d^{-1}	Faure et al. (2010)
$V_{DON,max}^{BA}$	Maximum DON uptake by bacteria	0.32	mmolN (10^{12} cell)$^{-1}$ d^{-1}	Faure et al. (2010)
$V_{NH_4,max}^{BA}$	Maximum NH_4 uptake by bacteria	0.32	mmolN (10^{12} cell)$^{-1}$ d^{-1}	Faure et al. (2010)
$V_{POP,max}^{BA}$	Maximum POP uptake by bacteria	0.01	mmolP (10^{12} cell)$^{-1}$ d^{-1}	Thingstad (1987)
$V_{DOP,max}^{BA}$	Maximum DOP uptake by bacteria	0.48	mmolP (10^{12} cell)$^{-1}$ d^{-1}	Thingstad (1987)
$V_{PO_4,max}^{BA}$	Maximum PO_4 uptake by bacteria	0.48	mmolP (10^{12} cell)$^{-1}$ d^{-1}	Thingstad (1987)
K_{POC}^{BA}	Half-saturation constant for POC	10.0	mmolC m^{-3}	Faure et al. (2010)
K_{DOC}^{BA}	Half-saturation constant for DOC	25.0	mmolC m^{-3}	/
K_{PON}^{BA}	Half-saturation constant for PON	0.50	mmolN m^{-3}	/
K_{DON}^{BA}	Half-saturation constant for DON	0.50	mmolN m^{-3}	/
$K_{NH_4}^{BA}$	Half-saturation constant for NH_4	0.15	mmolN m^{-3}	/
K_{POP}^{BA}	Half-saturation constant for POP	0.08	mmolP m^{-3}	/
K_{DOP}^{BA}	Half-saturation constant for DOP	0.08	mmolP m^{-3}	Leblanc et al. (2018)
$K_{PO_4}^{BA}$	Half-saturation constant for PO_4	0.02	mmolP m^{-3}	Campbell et al. (2013)
ε_{DIC}	fraction excretion of DIC	0.31	/	Faure et al. (2010)
ε_{NH_4}	fraction excretion of NH_4	0.50	/	Faure et al. (2010)
ε_{PO_4}	Fraction excretion of PO_4	0.50	/	Fraysse et al. (2013)
d_C	Fraction of C assimilated	0.92	/	Gerber and Gerber (1979)
d_N	Fraction of N assimilated	0.95	/	Faure et al. (2010)
d_P	Fraction of P assimilated	0.95	/	Fraysse et al. (2013)
$k_{C,zoo}$	Net C growth efficiency	0.40	/	Gerber and Gerber (1979)
$k_{N,zoo}$	Net N growth efficiency	0.44	/	Le Borgne and Rodier (1997)
$k_{P,zoo}$	Net P growth efficiency	0.37	/	Le Borgne (1982)
Q_{10}	Temperature coefficient	2.0	/	/
T_{rem}	Reference temperature for mineralization	20.0	°C	/

https://doi.org/10.5194/gmd-2020-41
Preprint. Discussion started: 18 May 2020

Geoscientific Model Development Discussions

k_{nit}	Nitrification rate	0.05	d^{-1}	Lacroix and Grégoire (2002)
T_{nit}	Reference temperature for nitrification	10.0	°C	/
K_{DO}	Half-saturation constant DO	30.0	$mmolO_2\ m^{-3}$	Tett (1990)
k_{diss}	Dissolution rate	10.9	d^{-1}	Gehlen et al. (2007)
k_{precip}	Fraction of PIC to POC	0.02	/	Marty et al. (2002)
K_C	Half-saturation constant of $CaCO_3$ precipitation	0.40	$(\mu mol\ kg^{-1})^2$	
$\left(\frac{O}{C}\right)_{PP}$	Ratio O:C for photosynthesis	1.0	/	/
$\left(\frac{O}{C}\right)_{nit}$	Ratio O:C for nitrification	2.0	/	/
$\left(\frac{O}{C}\right)_{uptNO_3}$	Ratio O:C for nitrate uptake	2.0	/	/
$\left(\frac{O}{C}\right)_{respBa}$	Ratio O:C for bacterial respiration	1.0	/	/

765